Spring 2006

Synthesis of polymeric nanocomposites in supercritical carbon dioxide

Hongta Yang
New Jersey Institute of Technology

ABSTRACT

SYNTHESIS OF POLYMERIC NANOCOMPOSITES IN SUPERCRITICAL CARBON DIOXIDE

by
Hongta Yang

Supercritical carbon dioxide has been of great interest in various areas of chemical science and engineering during the last decade. In this thesis, the properties of poly (methyl methacrylate) (PMMA)/silica nanocomposites with different surfactant and filler concentrations synthesized through in-situ polymerization in supercritical carbon dioxide were investigated. In addition, ferromagnetic nano-particles were synthesized and functionalized for the preparation of nanocomposites. The thermal stability and surface morphology of PMMA/iron oxide nanocomposites synthesized in supercritical carbon dioxide were first studied in the work.

The scanning electron microscopy micrographs show that higher surfactant concentration results in higher number density of polymeric nanocomposite particles and better dispersion of nano-particles in the polymeric composites. Higher concentration of silica nano-particles in the composites results in excessive particle agglomeration. The cause of agglomeration is due to the MPS molecules on different particles react with each other. A better thermal stability of the composites, as revealed by thermal gravimetric analyses and differential scanning calorimetry analyses, was observed due to the enhancement of the surfactant and filler interactions. Surprisingly, composites with PMMA grafted particles did not show an anticipated drastic improvement of the mechanical properties. This may result from the plasticizing effect of the stabilizer used in the dispersion polymerization.

SYNTHESIS OF POLYMERIC NANOCOMPOSITES IN SUPERCRITICAL CARBON DIOXIDE

by
Hongta Yang

A Thesis
Submitted to the Faculty of
New Jersey Institute of Technology
in Partial Fulfillment of the Requirements for the Degree of
Master of Science in Chemical Engineering

Otto H. York Department of Chemical Engineering

May 2006

APPROVAL PAGE

SYNTHESIS OF POLYMERIC NANOCOMPOSITES IN SUPERCRITICAL CARBON DIOXIDE

Hongta Yang

Dr. Chien-Yueh Huang, Thesis Advisor — Date
Assistant Professor of Chemical Engineering, NJIT

Dr. Robert Pfeffer, Committee Member — Date
Distinguished Professor of Chemical Engineering, NJIT

Dr. Zafar Iqbal, Committee Member — Date
Research Professor of Chemistry, NJIT

BIOGRAPHICAL SKETCH

Author: Hongta Yang

Degree: Master

Date: May 2006

Undergraduate and Graduate Education:

- Master of Science in Chemical Engineering,
  New Jersey Institute of Technology, Newark, NJ, 2006

- Bachelor of Science in Chemical Engineering,
  National Taiwan University, Taipei, Taiwan, 2001

Major: Chemical Engineering

Presentation:

Hongta Yang, Chien-Yueh Huang, and Marino Xanthos,
"Synthesis and Characterization of PMMA/Silica Nanocomposites,"
SPE ANTEC 2006.

To my beloved family

ACKNOWLEDGMENT

I would like to express my deepest appreciation to Dr. Michael Chien-Yueh Huang, who served as my thesis supervisor over the past two years, showing me different ways to approach and resolve the challenging research problems, and continuously giving me tolerance, encouragement and advice in my research work. With his broad knowledge, diligent working attitude and optimistic and kind spirit in daily life, Michael acted not only as an academic mentor, but also as good friend who impacted me in my future career. My special thanks go to Dr. Robert Pfeffer, and Dr. Zafar Iqbal for actively participating in my committee. I am grateful to the Society of Plastics Engineers for financial support of this research.

My appreciation to Dr. Wei-Kuo Lee, who guided me into the world of nanocomposites, is beyond my expression. My great thanks are given to Dr. Marino Xanthos, for his patient training in the extruder; Dr. Dongguang Wei, for his assistance and training in SEM; Dr. George Collins, Dr. Victor Tan and Dr. Michael Jaffe, for providing DSC, TGA, and DMTA instruments; and all those people who kindly gave me assistance in my research work. It would have been impossible to complete this work without their efforts. Finally, I am indebted to my fellow graduate students, Mr. Lining Zhu and Dr. Baohua Yue, who always helped me in the lab.

TABLE OF CONTENTS

TABLE OF CONTENTS
(Continued)

TABLE OF CONTENTS
(Continued)

Chapter **Page**

LIST OF TABLES

LIST OF FIGURES

LIST OF FIGURES
(Continued)

Figure **Page**

LIST OF FIGURES
(Continued)

Figure **Page**

LIST OF FIGURES
(Continued)

Figure **Page**

CHAPTER 1

INTRODUCTION AND OBJECTIVE

One major problem in the engineering application of polymers is their low stiffness and strength as compared with metals; the moduli are lower by around 100 times lower, and the strengths around 5 times. Addition of reinforcing particles to polymer to form a composite material is often used to offset these deficiencies. The employment of inorganic particle-filled composites not only can improve the physical properties of the materials such as the mechanical properties, thermal resistance, and chemical reagent resistance, but also can provide high-performance materials at a lower cost. This effect of fillers on the composite properties depends on the particle size, concentration, dispersion, and on the interaction with the matrix.

Nanocomposites make up a particular class of polymer composites that have recently garnered much attention, both in the academic fields as well as industry and government. Nanocomposites are a combination of two or more phases containing different compositions or structures where at least one of the phases is in the range of 10 to 100 nm. Not only can they provide the properties of traditional composites, but also they exhibit unique optical, electric, and magnetic properties. This growing class of materials can lead to reinforcement of a polymer without the undesirable property changes exhibited by large particulate filled system. Higher yield stress and Young's modulus in a nano-filled polymer composite compared to a micro-filled polymeric composite are expectable.

At present, organic/inorganic nanocomposites are prepared mainly via three methods:

(I) Sol–gel processing, which includes two approaches: hydrolysis of the metal alkoxides and then polycondensation of the hydrolyzed intermediates. Most of the interest in this method is concentrated on metal organic alkoxides since they can form an oxide network in organic matrices. This process provides a method for the preparation of inorganic metal oxides under mild conditions starting from organic metal alkoxides. This permits structural variations without compositional alteration. However, the formation of a cross-linking network of organic metal oxides makes a component difficult to process, and it is a disadvantage that circumscribed the application of this method.

(II) In-situ intercalative polymerization, which is a good method for the preparation of polymer/clay mineral hybrid or nanocomposites. Many other experiments reported on the syntheses of polymers in the interlayer space of clay. It is an effective method to prepare a polymer/clay composite which can provide high-performance materials at a relative low cost, but this method only adapts to clay minerals, which is also a significant disadvantage for its application.

(III) In-situ polymerization, which is a method where nanometer scale inorganic fillers or reinforcements are dispersed in the monomer first; then, this mixture is polymerized using a technique similar to bulk polymerization. It is obvious that the most important factors that affect the properties of composites are the dispersion and the adhesion at the polymer/filler interfaces. Inorganic particles may disperse homogeneously in the polymer matrices when they are premodified by a coupling agent. Furthermore, the resulting materials obtained by this method also can be easily processed since they have good flowing properties.

Several advanced polymeric nanocomposites have been synthesized with a wide variety of inclusion like metals, semiconductors, carbon nanotubes, and magnetic nano-particles. Many

attractive properties of polymers like non-corrosiveness, light weight, mechanical strength, and dielectric tenability can be utilized to make multifunctional materials.

The synthesis of polymeric composites usually involves solution chemistry, and the use of a large amount of organic solvents may raise serious air and water pollution concerns. Therefore, effective and green methods are of strong interest. There has been a continuing growth of interest in replacing conventional organic solvents with environmentally friendly supercritical fluids in chemical processes. Among them, supercritical carbon dioxide emerged as an excellent candidate due to its superb characteristics and properties: it is inexpensive, nontoxic, nonflammable, readily available, easily recycled, and as a solvent, it possesses both gas-like diffusivities and liquid-like densities and solvencies. Success in applying supercritical carbon dioxide as a solvent or processing medium has been found in various areas from the well-established supercritical extraction and separation to the relatively new engineered particle formation (Yeo et al., 1993; Reverchon et al., 1998). One area that has seen very much progress is polymer synthesis and processing (Reverchon et al., 2000).

From the aspect of processing, polymers can be fractionated, purified, impregnated or foamed by using supercritical carbon dioxide as a processing solvent. One of the recent interesting applications is synthesis of polymeric nanocomposites. In the area of polymer synthesis, following the seminal work of fluoropolymer synthesis in supercritical carbon dioxide (DeSimone et al., 1992), many common polymers were produced using supercritical carbon dioxide as the reaction medium. Dispersion polymerization, an important industrial process, is one of the most studied methods for polymer synthesis in supercritical carbon dioxide. It features an initially homogeneous solution reaction, where monomer, initiator and surfactant are all dissolved in a solvent. The system becomes heterogeneous once the polymer

solubility exceeds the solubility limit and polymer precipitates. The polymers produced by this method usually form spherical particles with a size range between 100nm to 10μm. Exploiting the favorable transport properties and controllability of the reaction in supercritical carbon dioxide, many important polymers using dispersion polymerization have been synthesized.

In search for materials with better mechanical and thermal properties, much emphasis has been given to the study of organic–inorganic nanocomposites. Poly (methyl methacrylate) (PMMA) is an important amorphous thermoplastic material with excellent transparency. However, its poor thermal stability and dynamic mechanical property at elevated temperatures restrain it from applications in high temperature environment. To improve the thermal stability and the mechanical property of PMMA, synthesized silica nano-particles have been employed in PMMA. In the study, a method based on the principles of dispersion polymerization in supercritical carbon dioxide was presented. The following research objectives and approaches will be implemented in this thesis:

(1) PMMA/Silica Nanocomposites Synthesized in Supercritical Carbon Dioxide

The first objective of this thesis is developing an efficient and clean polymeric nanocomposite synthesizing technology. A common filler material, silica nano-particles, was introduced into the high pressure vessel. Poly (methyl methacrylate) (PMMA) was synthesized in-situ via dispersion polymerization in supercritical carbon dioxide. It was found that this new method is efficient for the selected systems. Uniform encapsulation was obtained. In the system, polymer particles either coagulated or precipitated out as loose agglomerates. The morphology can be controlled by changing such process parameters as the fillers to monomer weight ratio and the concentration of the surfactant stabilizer. The chemical

characterization and thermal stability of nanocomposites with different process parameters were proposed.

(2) PMMA/Silica Nanocomposites Synthesized in Supercritical Carbon Dioxide Compared with Fabricated PMMA/Silica Nanocomposites

In comparison with PMMA homopolymer, silica enhanced the thermal stability of PMMA hybrid nanocomposites. Since the silica particles are hydrophilic, their surfaces need to be modified or pretreated with coupling agents to enhance the compatibility between the polymeric matrix and the particles. In this study, a new polymer grafting process through in-situ polymerization in supercritical carbon dioxide was employed. Thermal stability and mechanical properties of PMMA homopolymer, PMMA/silica melt mixing nanocomposites consisting of silica nano-particles, with and without surface grafting of PMMA, embedded in PMMA, and the PMMA/silica nanocomposites synthesized in supercritical carbon dioxide were studied.

(3) PMMA/Iron Oxide Nanocomposites Synthesized in Supercritical Carbon Dioxide

Magnetic nano-particles embedded in polymer matrices have excellent potential for electromagnetic device applications like electromagnetic interference suppression, spin-polarized devices, carriers for drug delivery, magnetic recording media, high-frequency applications, etc. Polymeric nanocomposites of PMMA doped with iron oxide nano-particles were synthesized in supercritical carbon dioxide with the employment of cross-linking agent. The polymer processing conditions were optimized to achieve good uniform dispersion of the nanoparticles in the polymer matrix. Surface characterization with scanning electron microscopy indicates that the iron nano-particles are embedded in the bulk; the surface mainly showed features associated with the polymer surface.

CHAPTER 2

LITERATURE REVIEW

Some previous works on the properties and applications of supercritical carbon dioxide, the use of supercritical carbon dioxide in polymer science and engineering, as well as the polymeric nanocomposite properties relevant to this work will be reported in this chapter.

2.1 Properties and Applications of Supercritical Carbon Dioxide

Every year, billion pounds of organic solvents are used worldwide as reaction media, dispersants, processing, and cleaning agents (Cooper et al., 1992). Reducing the emissions of hazardous volatile organic compounds has been vigorously pursued. To this account, an environmentally friendly solvent for chemical synthesis and processing to reduce the emissions has gained extensive interest.

Supercritical fluid is in a physical state under conditions above the critical temperature and critical pressure of a solvent. Fluid in such a state exhibits physicochemical properties between those of liquid and gas: liquid-like density and solvent strength, making it soluble to many organic compounds, while gas-like viscosity and diffusivity enhancing the transport ability. These therefore provide an easy route for otherwise difficult processes. In addition, thermodynamic, density, viscosity, and diffusivity can be tuned by process parameters such as pressure and temperature. Among many supercritical fluids been investigated, supercritical carbon dioxide, an inexpensive, non-toxic and non-flammable medium with an easily

accessible critical point—critical temperature at 31.1°C and critical pressure at 7.4 MPa, is the most salient in this category. These unique properties of supercritical carbon dioxide make it suitable of applications in such areas as organic synthesis, heterogeneous and homogeneous catalysis, and inorganic/metallorganic coordination chemistry (Johnston et al., 1989). Environmental, chemical, and economic advantages can be synergized by using supercritical carbon dioxide as a solvent (Sirard et al., 1991). One of the applications is the synthesis and processing of polymeric materials. DeSimone et al. (1992) first demonstrated the success of synthesizing fluorinopolymer in supercritical carbon dioxide to replace conventional solvents. This was a breakthrough initiating a series of related research. One interesting research area is to use supercritical carbon dioxide as a processing medium for the preparation of polymeric composites.

2.2 The Use of Supercritical Carbon Dioxide in Polymer Science and Engineering

Due to its liquid-like solvation power and gas-like diffusivity, supercritical carbon dioxide has attracted great interest as an alternative to organic solvent for the synthesis of polymeric composites. With a relatively low critical temperature and critical pressure, supercritical carbon dioxide is allowed for more economical operation. After depressurization, supercritical carbon dioxide can be easily released or recycled. Although various supercritical technologies have been developed, rapid expansion of supercritical solutions and supercritical antisolvent process are two most widely used techniques for synthesis of polymeric composites (Christain et al., 1993).

2.2.1 Rapid Expansion of Supercritical Solutions (RESS)

In a typical RESS process, polymers material is dissolved in supercritical carbon dioxide and the solution is atomized through a nozzle. The quick supersaturation due to volume expansion results in precipitation of polymer material in the form of particles of small size and narrow size distribution. The polymer material may precipitate onto inorganic particles to form polymeric composites. The drawback of the RESS technique is that only a few groups of polymers dissolve in supercritical carbon dioxide, which greatly restricts its application. To overcome the low solubility of many materials, cosolvent is often added to facilitate solid dissolution in supercritical carbon dioxide.

Several researchers have explored drug/polymer coprecipitation with RESS process. Tom et al. (1994) investigated the coprecipitation pyrene with PLA to form composite particles in a RESS process. Pyrene solution and PLA dissolved in supercritical carbon dioxide with cosolvent CHClF2 were sprayed into the expansion chamber and precipitate out. Kim et al. (1996) investigated the coprecipitation of naproxen with PLA. PLA and naproxen were extracted into supercritical carbon dioxide and then sprayed the solution through a nozzle for precipitation.

The RESS process was also used to encapsulate inorganic particles by Mishima, et al. (1998). In the RESS process the polymer and the inorganic particles are both dissolved in supercritical carbon dioxide with or without a cosolvent. The solution is then released from a nozzle, generating polymeric microparticles. In RESS, the rapid de-pressurization of the supercritical solution causes a substantial lowering of the solvent power of supercritical carbon dioxide leading to very high super-saturation of the solute, precipitation, nucleation and particle growth.

However, the application of the RESS process is severely limited by the fact that polymers, in general, have very limited solubility in supercritical carbon dioxide at temperatures below 80°C (O'Neill et al., 1998). Also, the operating pressure in RESS is usually above 200 bars so that it is less attractive economically.

Tsutsumi et al. (1995; 2001) used a combination of the RESS process and a fluidized bed for the synthesis of polymeric composites. In this research, a solution of polymer material in supercritical carbon dioxide is sprayed into the fluidized bed of inorganic particles to synthesize polymeric composites. However, inorganic particles less than 30-50 μm are very difficult to fluidize. Hence this method cannot be easily used to synthesize polymeric composites with ultrafine particles

Pessey et al. (2000; 2001) demonstrated the use of a supercritical fluid process to synthesize polymeric composites. His work involved the thermal decomposition of an organic precursor and the deposition of copper onto the surface of core particles in supercritical carbon dioxide under conditions of temperature up to 200°C and pressure up to 19MPa. However, the methods are less attractive from the point of view of safety and cost.

Recently, Wang et al. (2004) developed a modified RESS by using a solution of polymer in supercritical carbon dioxide and showed that the composites of glass particles with PVCVA and HPC were successfully achieved using this technique. The use of a co-solvent could improve the solubility of polymers and also affected the degree of crystallinity of the polymer. The extraction and precipitation technique took advantage of the properties of a supercritical solution in that the polymer would nucleate, grow and deposit on the inorganic particle surfaces due to changes in its solubility caused by the adjustment of temperature and pressure.

2.2.2 Supercritical Antisolvent Process (SAS)

For materials that do not dissolve in supercritical carbon dioxide, SAS is usually applied, in which supercritical carbon dioxide acts as an antisolvent to induce the nucleation and precipitation of a solute. In this process, materials are dissolved or suspended in an organic solvent that is miscible with supercritical carbon dioxide. The solution or suspension is then sprayed into supercritical carbon dioxide through an atomizer. An instantaneous supersaturation facilitated by fast mutual mass transfer leads to precipitation of dissolved material in the form of particles. In the SAS process, the particle size, size distribution, morphology, and crystallization are strongly dependent on the mass transfer, with such variables as temperature, pressure, solution concentration, supercritical carbon dioxide flow rate, solution flow rate, and nozzle design.

Wang successfully developed SAS technology for synthesis of nanocomposites with Eudragit (Wang et al., 2003). A suspension of silica particles in a polymer solution was sprayed into supercritical carbon dioxide through a capillary tube. The subsequent mutual diffusion between supercritical carbon dioxide and polymer solution droplets resulted in high degree of supersaturation, and that causes a heterogeneous polymer nucleation induced by the phase transition, with the silica nano-particles acting as nuclei. Thus the particles were individually encapsulated in polymer with very little agglomeration. For 600nm particles the surface morphology and microstructure of the polymeric composites were controlled by adjusting the ratio of polymer to silica particles. In a separate research, hydrocortisone particles/ PLGA composites were successfully synthesized in the SAS coating process.

SAS is also used for coprecipitation of a drug substance and a polymer. Falk et al. (1997) successfully synthesized the formation of drug/polymer composites with the SAS process. In

the research, a solution of drugs and PLA were sprayed into supercritical carbon dioxide as an antisolvent to induce co-precipitation of drug and PLA. However, coprecipitation of drug and polymer requires that both be dissolved in a suitable solvent which is challenging for the two solutes, as they have different thermodynamic properties and undergo different precipitation pathways. An important feature of the SAS process is that the organic solvent can be almost completely removed by simply flushing with pure supercritical carbon dioxide. Thus, dry particles are produced after a supercritical carbon dioxide extraction step following organic solution injection.

2.3 Properties of PMMA/Silicate Nanocomposites

Polymeric nanocomposite, finding applications in various important industries, such as biomedical industry, consists of a polymer matrix and one or more dispersed phases with nano-scale features. The incorporation of nano-particles into polymer matrix is often intended to improve the mechanical, thermal or electrical properties of the composite material. The confinement of polymer chains in nano-scale brings up various interesting phenomena that are not observed in regular macroscopic composites. The role of embedded nano-particle in polymeric composites to external stimuli is still open to investigation. In one possible scenario, only the mobility of the polymer chains around the nano-particle surface is affected which results in solely near-field effect. On the other hand, the nano-particles may affect long-range collective motions of the polymers or form cross-linking that enhances the mechanical properties.

Conventional preparation methods for composites usually are involved with physical mixing of polymers and fillers through such operation as blending, extrusion, or solution

casting. However, nano-particles may have very high cohesive energy to form agglomerates; processes based on simple mixing are not effective in breaking up the agglomerates to form homogeneous nanocomposite.

In the last decade, a few new approaches were investigated to make polymer inorganic composites via in-situ polymerization. Von Werne et al. (2001) modified the surface of silica nano-particles with initiators for atom transfer radical polymerization (ATRP) where in polymer chains are tethered on particle surfaces and form a layer. Bourgeat-Lami et al. (2004) investigated silica styrene nanocomposites synthesized with dispersion polymerization in ethanol.

Recently, supercritical processing has attracted growing interests for polymer nanocomposite fabrication due to its environmental friendliness, simple product collection, and down-stream processing. In one approach, organic precursors were impregnated into the polymer matrix in supercritical carbon dioxide and then decomposed into inorganic particles after heating to form composites. The resultant nano particles or products are restrained from agglomeration in polymer matrices. Using this approach, platinum, copper, silver and iron nano-particles have been embedded in a variety of polymer matrices with, unfortunately, higher polydispersity (Wang et al., 2002).

Poly (methyl methacrylate) (PMMA) is an important amorphous thermoplastic material with excellent transparency. However, its poor thermal stability and dynamic mechanical properties at elevated temperatures restrain it from applications in high temperature environment. To improve the thermal stability and the mechanical properties of PMMA, modified clay and synthesized silica nano-particles have been commonly employed in PMMA

hybrid composites. The properties of PMMA/fillers nanocomposites were investigated as following.

2.3.1 Syntheses and Characterization of PMMA/Clay Nanocomposites

Several researchers have investigated PMMA/Clay nanocomposites. Yeh et al. (2002) studied a series of polymer/clay nanocomposite materials that consisted of PMMA and layered montmorillonite (MMT) clay. These composites were prepared by effectively dispersing the inorganic nanolayers of MMT clay in an organic PMMA matrix via in-situ thermal polymerization. MMA monomers were first intercalated into the interlayer regions of organophilic clay hosts followed by a typical free radical polymerization.

In Okamoto's works (2001; 2002; 2003), via in-situ intercalative free-radical polymerization, PMMA/clay nanocomposites from lipophilized smectic clays were prepared. . Under some conditions, the intercalative nanocomposites exhibited flocculation because of the hydroxylated edge-edge interaction of silicate layers. The nanocomposites had higher storage modulus and higher glass transition temperature compared to the systems without clay.

In Yue's research (2004), a series of polymer/clay nanocomposites consisting of organic PMMA and inorganic montmorillonite (MMT) clay platelets were successfully prepared by the effective dispersion of nanolayers of the MMT clay in the PMMA frame-work through both in-situ emulsion polymerization and solution dispersion. As a comparison of the anticorrosion performance, polymer/clay nanocomposites prepared by in-situ emulsion polymerization, with better dispersion of the clay platelets in the polymer matrix, exhibited better corrosion protection in the form of a coating on a cold-rolled steel coupon than that

prepared by solution dispersion. The latter showed a poor dispersion of the clay nanolayers according to a series of electrochemical corrosion measurements,.

Han et al. (2005) synthesized the PMMA/sodium montmorillonite (Na-MMT) nanocomposites utilizing a macroazoinitiator (MAI). To induce the intergallery polymerization of methyl methacrylate (MMA), the MAI containing a poly (ethylene glycol) (PEG) segment was intercalated between the lamellae of Na-MMT and swelled with water to enhance the diffusion of MMA into the gallery. The PMMA/Na-MMT nanocomposite prepared by intergallery polymerization showed a distinct enhancement of its thermal properties.

Stadtmueller et al. (2005) investigated in-situ bulk polymerization of PMMA/clay nanocomposites which was initiated with a benzoyl peroxide/amine redox couple at room temperature. This was accomplished with a synthesized cationic molecule, containing an aliphatic chain and an aromatic tertiary amine, which was ion exchanged onto the clay surface in order to control the rate of intragallery polymerization relative to that of extragallery polymerization.

In Zhang's work (2003), PMMA/clay nanocomposites were prepared with reactive modified clay and nonreactive clay via γ-ray irradiation polymerization. With reactive modified clay, exfoliated PMMA/clay nanocomposites were obtained, and with nonreactive clay, intercalated PMMA/clay nanocomposites were obtained. PMMA extracted from PMMA/clay nanocomposites synthesized by γ-ray irradiation had higher molecular weights and narrow molecular weight distributions. The enhanced thermal properties of the PMMA/clay nanocomposites were characterized by thermogravimetric analysis and differential scanning calorimetry. The improved mechanical properties of PMMA/clay were

also characterized. The enhancement of the thermal properties of the PMMA/clay nanocomposites with reactive modified clay was formed much more obvious than that of the PMMA/clay nanocomposites with nonreactive clay.

Meneghetti et al. (2004; 2005; 2006) modified the surface of clay (montmorillonite, MMT) with a zwitterionic surfactant, octadecyl-dimethyl betaine (C18DMB). Polymer-clay nanocomposites constitute a new class of materials in which the polymer matrix is reinforced by uniformly dispersed inorganic particles (usually 10 wt. % or less) with at least one dimension in the nanometer scale. Nanocomposites exhibit improved properties when compared to pure PMMA homopolymer or conventional composites, such as enhanced mechanical and thermal properties, reduced gas permeability, and improved chemical stability.

In Zeng's study (2001; 2003), polymer/clay nanocomposite foams using carbon dioxide as the foaming agent were prepared. It was found that clay nano-particles served as an efficient nucleation agent. The nucleation efficiency was affected by both clay dispersion and polymer-clay-CO_2 interaction. These foams exhibited good combination of stiffness, toughness, weight saving, and dimension stability.

Jash et al. (2005) synthesized the nanocomposites of PMMA with layered silicates prepared by bulk polymerization. The thermal and fire stabilities of the various organically-modified clay nanocomposites were evaluated.

Xu et al. (2005) synthesized P(MMA-co-AN)/Na-MMT nanocomposites through emulsion polymerization with pristine Na-MMT. The nanocomposites exhibited enhanced storage moduli relative to the neat copolymer. The onset of the thermal decomposition of the nanocomposites shifted to a higher temperature as the clay content increased. By calculating areas of tan δ of the nanocomposites, the nanocomposites show more solid-like behavior with

the increase in clay content. The dynamic storage modulus and complex viscosity also increased with clay content. The complex viscosity showed shear-thinning behavior with higher clay content. The Young's moduli of the nanocomposites are higher than that of the neat copolymer and they increase steadily with the silicate content, as a result of the exfoliated structure at high clay content.

2.3.2 Synthesis and Characterization of PMMA/Silica Nanocomposites

Shen et al. (1999) studied the organic-inorganic hybrid nanocomposite materials of PMMA and organically-modified silica systems. These were prepared via melt intercalation with variation of tacticity and molecular weight as the main molecular variables. The degradation temperature of the PMMA/silica hybrid is higher than that of PMMA alone, or a physical mixture of PMMA and silica under an air or a nitrogen flow.

Choi et al. (2001; 2003) synthesized polymer/silica nanocomposites using potassium persulfate (KPS) in the presence of silica and 2-acrylamido-2-methyl-1- propanesulfonic acid (AMPS) without exterior redox co-catalysts at a room temperature. Poly (acrylonitrile) (PAN)/silica nanocomposites showed an exfoliated structure Poly (methyl methacrylate) (PMMA)/silica nanocomposite on the other hand showed an intercalated structure. Polymers recovered from the nanocomposites synthesized at a room temperature had high isotactic configurations compared to bulk polymers. The dipole-dipole interaction between monomers and silica surface might make the lamella of monomers to form on the silica surface and produced polymers with more isotactic configurations.

Mori et al. (2004) developed a synthetic method of PMMA/silica nanocomposites with well-segregated PMMA and silica domains. To obtain the nanocomposite, a

PMMA-block-PHEMA film was soaked into a pyridine/m-xylene/perhydropolysilazane (PHPS) mixture and calcinated at 90 °C under steam. PHPS was homogeneously introduced into the film and selectively converted to silica in PHEMA microdomains of the PMMA-block-PHEMA film.

Luna-Xavier et al. (2002, 2004) used 2, 2′-azobis (isobutyramidine) dihydrochloride (AIBA) as a cationic initiator to generate positively charged polymers, and promoted interaction of these polymers with the negatively charged surface of colloidal silica particles in aqueous solution. Three different synthetic routes were investigated. In a first route, emulsion polymerization of MMA, initiated by AIBA, was performed directly in an aqueous suspension of the silica beads using a non-ionic polyoxyethylenic surfactant. In a second route, AIBA was first adsorbed on the silica surface, and the free amount of initiator was discarded from the suspension. The silica-adsorbed AIBA adduct was suspended in water with the help of a surfactant to initiate the emulsion polymerization of MMA. In a third route, cationic PMMA particles were synthesized separately and subsequently adsorbed on the silica surface. In all their approaches, the colloidal nanocomposites were shown to exhibit a raspberry-like morphology.

Chen et al. (2004) prepared waterborne raspberry-like PMMA/silica nanocomposites via a free radical copolymerization of MMA monomer with 1-vinylimidazole (1-VID) in the presence of ultrafine aqueous silica sols. The acid-base interaction between hydroxyl groups of silica surfaces and amino groups of 1-VID was strong enough for promoting the formation of long-stable PMMA/silica nanocomposite particles when 1-VID as auxiliary monomer was used.

PMMA/silica nanocomposites are prepared by solution polymerization by Yang et al. (2004) and the resulted materials are subjected to characterization and evaluation of the thermal, mechanical, and fire properties. It shows that both (3-acryloxypropyl) methydimethoxysilane and (3-acryloxypropyl) trimethoxysilane can serve as reagents for the surface modification of silica, while APTMOS performed better than APMDMOS for the modification of the silica surface. Mechanical properties of PMMA/silica nanocomposites prepared by solution blending showed decreased tensile strength and elongation at break, while materials from solution polymerization performed better than PMMA itself. Moreover, all prepared samples have shown improved thermal stabilities versus PMMA.

Salem et al. (2005) performed reversible addition-fragmentation chain transfer (RAFT) polymerizations were performed in the presence of organically modified silica and successfully prepared PMMA/silica nanocomposites. The polymers had well-defined molecular weights and low polydispersities, as expected from RAFT polymerizations.

Qi et al. (2006) investigated the poly(butyl acrylate)/poly(methyl methacrylate) (PBA/PMMA) core-shell particles embedded with nanometer-sized silica particles, The nanocomposites were prepared by emulsion polymerization of butyl acrylate (BA) in the presence of silica particles preabsorbed with 2,2′-azobis(2-amidinopropane)dihydrochloride (AIBA) initiator and subsequent MMA emulsion polymerization in the presence of PBA/silica composite particles. The morphologies of the nanocomposites showed that the critical amount of AIBA added to have stable dispersion of silica particles increased as the pH of the dispersion medium increased.

Kurian et al. (2006) modified the surface of silica by organic surfactants, and the nature of surfactant-matrix enthalpic interactions on polymer/silica nanocomposites have also been

systematically investigated. Modified silica were prepared and used in turn to fabricate PMMA/silica nanocomposites via static melt intercalation. The nanocomposites were seemingly dependent on surfactant chain length, with the shortest surfactant providing the most significant disruption of the clay tactoids.

Rhee et al. (2002) synthesized the PMMA/silica nanocomposites containing calcium salt through the sol-gel method. MMA was co-polymerized with 3-(trimethoxysilyl)propyl methacrylate and then co-condensed with tetraethyl orthosilicate and calcium nitrate tetrahydrate. The low crystalline hydroxyl carbonate apatite was successfully formed on its surface after soaking in simulated body fluid for 1 week at 36.5 °C. It implies that this nanocomposite may be used as a bioactive bone substitute or filler for the PMMA bone cement.

Takahashi found that PMMA works as an efficient host binder material and that a refractive index modulation of 0.005 is possible with PMMA. It is also shown that silica nano-particles can be uniformly dispersed in a monomer-PMMA mixture to form a volume holographic grating with a refractive index modulation of 0.005 (TakaHashi et al., 2005).

Wang et al. (2005) investigated the nanocomposites from PMMA/silica using non-hydrolytic sol-gel process. Silicic acid and zirconium oxychloride ($ZrOCl_2 \cdot 8H_2O$) were used as the precursors of silica, respectively. The nano-scaled silica particles were uniformly distributed in and covalently bonded to the PMMA host matrix without macroscopic organic-inorganic phase separation, and this was confirmed by solvent extraction experiments. It was found that the transmittance of the nanocomposite films in the visible region remained above 95% even at 20 wt. % inorganic content and increased proportionally with decreasing

inorganic content. The thermal stability and the thermal decomposition kinetics of the composites were also studied.

Huang et al. (2000; 2001) investigated PMMA/silica nanocomposites prepared by in-situ suspension polymerization and emulsion polymerization. For the suspension polymerization, the silica were dispersed individually in water, and they are adsorbed on the surface of monomer droplets. For the emulsion polymerization, the nanocomposite was obtained by adding an aqueous dispersion of silica into the polymer emulsion. Compared to a PMMA homopolymer, the nanocomposites prepared by these methods display higher glass transition temperatures and thermal degradation temperatures.

Di et al. (2006) found that exfoliated nanocomposites with very high silica contents could be used as nanoadditives or masterbatches to prepare various nanocomposites by simple blending without the necessity to begin from scratch. The exfoliation remained stable to subsequent thermal processing. The storage modulus of PMMA/silica nanocomposite was higher than that of neat PMMA in the glassy region below the glass transition temperature of PMMA.

Kashiwagi et al. (2003) synthesized PMMA/silica nanocomposites by in-situ polymerization of MMA with colloidal silica (ca. 12 nm) to study the effects of nano-scale silica particles on the physical properties and flammability properties of PMMA. The addition of nanosilica particles (13% by mass) did not significantly change the thermal stability, but it made a small improvement in modulus, and it reduced the peak heat release rate roughly 50%.

Yue et al. (2005) synthesized the macroporous monoliths consisting of silica nanoparticles embedded in PMMA in supercritical carbon dioxide. Well-dispersed silica nano-particles, pretreated with functional 3-(trimethoxysilyl)-propyl methacrylate (MPS), were to form

colloidal PMMA nanocomposites followed by a sol-gel transition forming interconnected structures resulting in micron-sized pores.

CHAPTER 3

EXPERIMENTAL SECTION

3.1 Materials

3.1.1 Chemicals for PMMA/Silica Nanocomposites

The reagents used for silica particle synthesis, including tetraethyl orthosilicate (TEOS, 98%), ammonium hydroxide (NH_4OH, 99.5%), and ethanol (99.5%), were all purchased from Sigma-Aldrich. 3-(trimethoxysilyl) propyl methacrylate (MPS, 99%) was obtained from Fisher Scientific. Chemicals used for dispersion polymerization in supercritical carbon dioxide include methyl methacrylate (MMA, 99%), surfactant stabilizer poly (dimethylsiloxane) methacrylate (PDMS-MA, 99%) as shown in Scheme 3.1, and initiator 2, 2'-azobisisobutyronitrile (AIBN, 98%). The chemicals were obtained from Sigma-Aldrich. Liquefied carbon dioxide with 99% purity was purchased from Matheson. Laboratory grade poly (methyl methacrylate) (PMMA, Mw. =150,000) was also obtained from Sigma-Aldrich. All the chemicals were used as received.

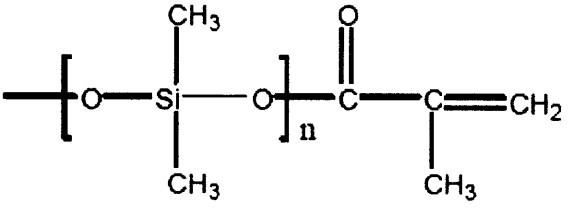

Scheme 3.1 Molecular structure of surfactant PDMS-MA.

3.1.2 Chemicals for PMMA/Iron Oxide Nanocomposites

The reagents used for iron oxide particle synthesis, including iron (II) chloride tetrahydrate ($FeCl_2 \cdot 4H_2O$, 99%), iron (III) chloride hexahydrate ($FeCl_3 \cdot 6H_2O$, 97%), dodecanedioic acid

(99%), perchloric acid (70%), ammonium hydroxide (NH_4OH, 99.5%), acetone (99.8%), and methanol (99.8%), were all purchased from Sigma-Aldrich. 2-Aminoethyl methacrylate hydrochloride (AEMA, 90%), N, N,-dimethyl formamide (DMF, 99.8%), and tetrahydrofuran (THF, 99%) were used for surface functionalization. They were also purchased from Sigma-Aldrich and used without further purification. Chemicals used for dispersion polymerization in supercritical carbon dioxide include methyl methacrylate (MMA, 99%) (Sigma-Aldrich), surfactant stabilizer poly (dimethylsiloxane) methacrylate (PDMS-MA, 99%) (Sigma-Aldrich), initiator 2, 2'-azobisisobutyronitrile (AIBN, 98%) (Sigma-Aldrich), and ethylene glycol dimethacrylate (EDMA, 98%) (Sigma-Aldrich). Liquefied carbon dioxide with 99% purity was purchased from Matheson.

3.2 Synthesis of PMMA/Silica Nanocomposites

3.2.1 Synthesis of Silica Nanoparticles

Silica nano-particles were synthesized according to the process described by Stober et al.. In the process, TEOS was hydrolyzed to form silica particles in ethanol with a catalyst, NH_4OH, at room temperature as shown in Scheme 3.2. Monodisperse spherical particles of controlled sizes, ranging from tens to thousands of nanometers, were synthesized in our lab by changing the concentrations of reactant and catalyst. In the synthesis, TEOS (46.8 ml) were hydrolyzed to form silica particles in ethanol (300 ml) with the catalyst, NH_4OH (28.2 ml), at room temperature over a period of two days. Spherical particles with a narrow size distribution (an average size of 75 nm in diameter) and smooth surface were obtained in ethanol. Silica particles synthesized by the above method are hydrophilic, with hydroxide groups on the silica particle surface.

Hydrolysis:

$$Si(OR)_4 + H_2O \rightleftharpoons (HO)Si(OR)_3 + ROH$$

$$(HO)Si(OR)_3 + H_2O \rightleftharpoons (HO)_2Si(OR)_2 + ROH$$

$$(HO)_2Si(OR)_2 + H_2O \rightleftharpoons (HO)_3Si(OR) + ROH$$

$$(HO)_3Si(OR) + H_2O \rightleftharpoons Si(OH)_4 + ROH$$

Alcohol Condensation (Alcoxolation):

$$\equiv Si\text{-}OR + HO\text{-}Si\equiv \rightleftharpoons \equiv Si\text{-}O\text{-}Si\equiv + ROH$$

Water Condensation (Oxolation):

$$\equiv Si\text{-}OH + HO\text{-}Si\equiv \rightleftharpoons \equiv Si\text{-}O\text{-}Si\equiv + HOH$$

Net Reaction:

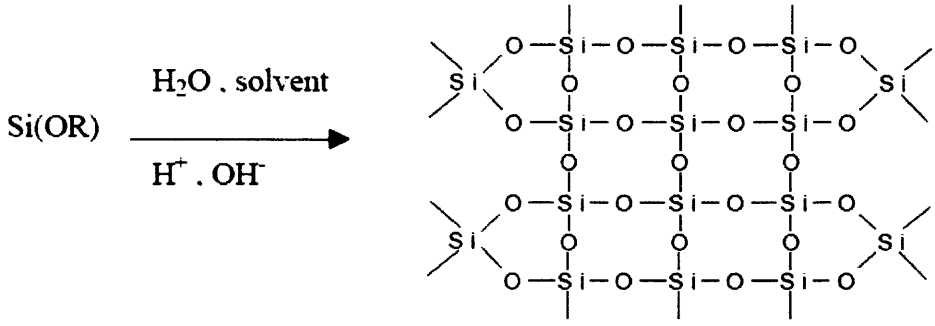

Scheme 3.2 Synthesis of silica particles.

3.2.2 Modification of Silica Nanoparticles

To make the particle surfaces hydrophobic, we followed a well-established surface treatment by adding coupling agent, MPS, into the silica nano-particle dispersion and stirring the

solution at room temperature for two more days. MPS reacted with the hydroxide groups to turn the silica surface from hydrophilic into hydrophobic and provided methacrylate terminal groups for polymer grafting, as shown in Scheme 3.3. The solution containing modified silica nano-particles were then dialyzed with cellulose membrane against ethanol to eliminate the ammonia and free MPS molecules.

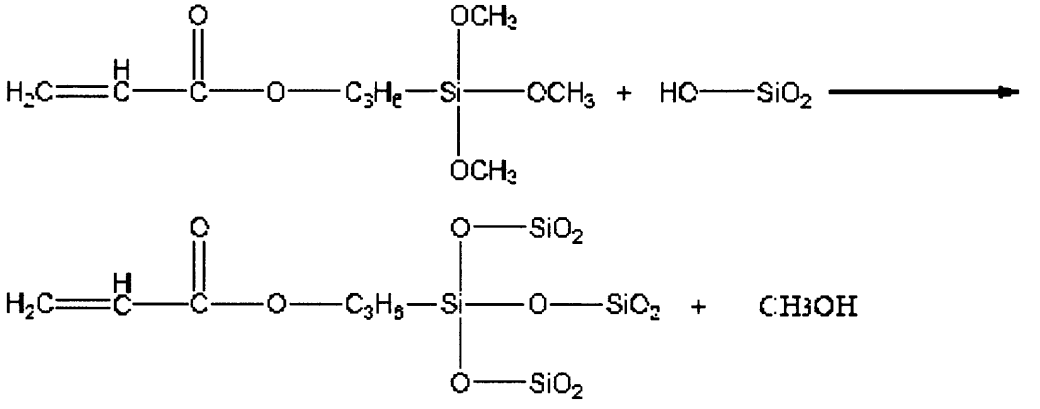

Scheme 3.3 Surface modification of hydrophilic silica particles with MPS.

3.2.3 Composites Synthesis via Polymerization in Supercritical Carbon Dioxide

The polymerization system setup, which consists of a 25-ml Parr Instruments high-pressure reactor vessel with two sapphire windows at both ends, is shown in Scheme 3.4. There are four openings on the reactor sidewalls which are separately designed for the thermocouple, pressure transducer and safety discs, inlet for reactant and carbon dioxide injection, and outlet for carbon dioxide. The thermocouple and pressure transducer were connected to Watlow panel meters for digital readout. The reactor pressure was manually controlled by pumping or releasing carbon dioxide through the inlet/outlet. Heating was supplied with electric silica rubber wrapped around the reactor and the temperature was controlled by changing the voltage applied to the heating tape.

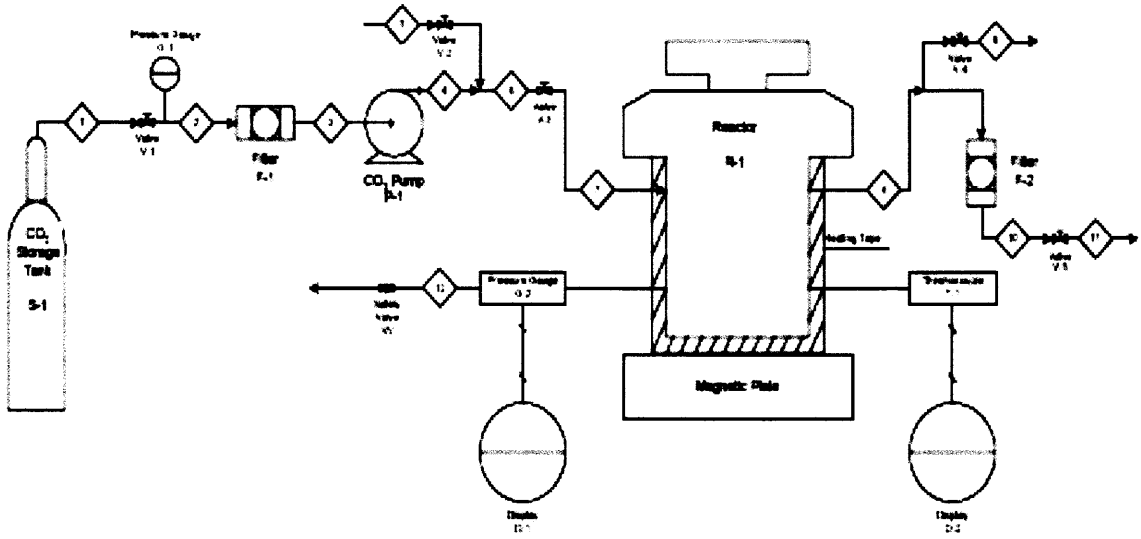

Scheme 3.4 Schematic diagram of the high-pressure reaction system used in the study.

The synthesis of PMMA/silica nanocomposites by in-situ polymerization was conducted in a high pressure batch reactor. During the polymerization, AIBN acts as free-radical initiator and PDMS-MA functions as a surfactant stabilizer. In a typical batch, MMA, PDMS-MA, AIBN, and silica nano-particles were premixed in a sonicator (SC-101TH) for 1 hour before loaded into the reactor. After the premixed chemicals were loaded, the reactor was purged with liquefied carbon dioxide by a Haskel Air Driven pump at room temperature until the pressure reached 13790 MPa. All valves of the reactor were then closed. Before the reaction started, the monomer, surfactant, and initiator were all dissolved in carbon dioxide, while the silica particles were suspended in the reactor vessel with magnetic stirring. As the pressure reached 27580 MPa, the vessel was then heated to 65°C to initiate the in-situ polymerization. The batch reactor remained closed during the experiment and a pressure drop of 500~1000 MPa due to polymerization-induced volume shrinkage was commonly observed after the reaction completed. Each experiment was run for 24 hours, after that carbon dioxide was released and the reactor was cooled down to room temperature for sample collection.

3.2.4 Composites Synthesis via Melt Mixing

The melt mixing composites were prepared using a 15 mm diameter co-rotating twin-screw extruder (APV MP-2015). The temperatures of the extruder were set at 190°C, and the operating temperatures were measured as follows: the temperature of 1_{st} zone near hopper was 190°C, the temperature of 2_{nd} zone was 176°C, and the die temperature was 107°C. Feed rate was 0.295 g/min, the screw speed was 30 rpm, and the residence time was 60 seconds. Neat PMMA, PMMA/unmodified silica nano-particles, and PMMA/surface modified silica nano-particles, respectively by rolling the given ingredients in a bag for about 10 min before being charged into the hopper of the extruder. Mixing time was counted from the time when the materials were loaded into the extruder.

3.3 Synthesis of PMMA/Iron Oxide Nanocomposites

3.3.1 Synthesis of Ferrofluid

The synthesis of iron oxide nano-particles (Fe_3O_4) was based on a procedure reported by Wooding (Wooding, et al. 1991), in which coprecipitation of Fe(II) and Fe(III) salts by NH_4OH at 60 °C was followed by an addition of surfactants. Two modifications were made from Wooding: the use of a room temperature precipitation temperature and a doubling of the amount of added ammonium hydroxide. In a typical synthesis to obtain iron oxide nano-particles, 6 g of $FeCl_3 \cdot 6H_2O$ and 2.1 g of $FeCl_2 \cdot 4H_2O$ were dissolved in 100 ml of water with vigorous stirring, and 13 ml of 28% (w/w) NH_4OH was added. Additional 2.5 g of dodecanedioic acid was added to the suspension and stirred at 90 °C for 30 min.

3.3.2 Synthesis of Surface Modified Magnetic Iron Oxide Particles

The above water-based iron oxide suspension was then cooled slowly to room temperature and 8 ml of 2 M perchloric acid was added. A black gum-like solid formed immediately that settled over a magnet, leaving a clear supernatant liquid with a thick surface scum of excess surfactant. The liquid was decanted, the black residue was washed several times with acetone and MeOH, and the precipitates were isolated from the solvent by magnetic decantation. This washing-decantation procedure was repeated 5 times to remove the excess dodecanedioic acid used for the primary layer, and the removal was confirmed by gas chromatography by the lack of dodecanedioic acid in the magnetic decantation supernatant. Finally, the precipitates were vacuum dried for 48 hours to obtain the surfactant-coated magnetic particles. The magnetic particles synthesized by the above method are hydrophilic. To make the particle surface hydrophobic, a surface treatment was followed by adding 40 mg of 2-aminoethyl methacrylate hydrochloride (AEMA) and 30 ml of N, N,-dimethyl formamide (DMF) to 10 mg of magnetic particles. The mixture was refluxed at 153 °C for 48 hours, and then the solution was cooled down to 65 °C. After the reflux, the solution was washed by tetrahydrofuran (THF) with nano-filter to collect the magnetic nano-particles with an average size of 35nm in diameter.

3.3.3 Synthesis of PMMA/Iron Oxide Monoliths in Supercritical Carbon Dioxide

Composite synthesis with in-situ polymerization was conducted in the high-pressure reaction vessel. During polymerization, 1.5 ml of methyl methacrylate (MMA), 0.15 g of magnetic nano-particles, 0.04g of 2, 2'-azobisisobutyronitrile (AIBN) which acts as free-radical initiator, 0.3g of poly (dimethyl siloxane) methacrylate (PDMS-MA) which functions as a surfactant stabilizer, and 0.1 g of ethylene glycol dimethacrylate (EDMA) which plays as

cross-linking agent, were premixed and charged into the reactor followed by purging with low-pressure carbon dioxide. After purging, liquefied carbon dioxide was pumped into the reactor at room temperature until the pressure reached 13790 MPa, the vessel was then heated to 65°C to initiate the free-radical polymerization. Keep the reaction temperature at 65°C and the vessel pressure at 27580 MPa for 24 hours. A chalk-like PMMA monolith with 10 % of iron oxide was collected.

3.4 Material Characterization Methods

The physical and chemical properties of the synthesized particles or polymeric nanocomposites are determined by a series of characterization methods as follow.

A. Scanning Electron Microscopy (SEM)

Leo 1530VP® SEM was employed to examine the surface morphology and microstructure of the polymer materials. The sample was stick to the top of the tape on the sample holder, and then fixed with compressed air. All the samples underwent a carbon thin-film coating with BAL TEC MED 20 HR Sputtering Coater before the microscopic characterization. The coating was conducted at high vacuum ($<2x10^{-5}$ bar). All the microscopies are performed under 1kV, with a working distance range of 3 to 5mm.

B. Differential Scanning Calorimetry (DSC)

DSC was used to measure the glass transition temperature of the synthesized polymeric nanocomposites. The glass transition temperatures of the samples were measured by DSC. The reported glass transition temperature is between 110°C to 120°C for PMMA (Sigma-Aldrich MSDA data). Based on the glass transition temperature, the testing temperature ranges have been set as 0~220°C for all samples. The equipment models used in

this work is TA-Q100® DSC. The DSC measurements for the samples were performed at a heating rate of 10°C/min; while the DSC for the samples were conducted with a heating-cooling-heating cycle, with a heating rate of 10°C and a cooling rate of 10°C, respectively.

C. Thermogravimetric Analysis (TGA)

TA-Q50® TGA was employed to investigate the thermal stability of the composites. The decomposition temperature and the weight percentage of silica nano-particles in the composites were measured by TGA. The testing temperature ranges have been set as 25~475°C for all samples. The TGA measurements were performed at a heating rate 10°C/min, under the dry nitrogen atmosphere with the nitrogen flow rate at 40ml/min.

D. Dynamic Mechanical Thermal Analysis (DMTA)

Dynamic mechanical thermal analysis (DMTA, TA Q800) was employed to measure T_g and the moduli in a tension mode. All samples were first compressed into sheets and were cut into a dimension of 15×7.25×0.4 mm^3. These specimens were cooled to 20°C first, held for 5 min, and heated to 130°C at 10°C/min. A dynamic force of 0.1 N oscillating at 1 Hz and amplitude of 0.01 μm was employed. Loss tangent (tan δ) was used to evaluate the glass transition temperature; the peaks of tan δ curves were taken as the T_g.

E. Gel Permeation Chromatography (GPC)

Gel permeation chromatography (GPC), performed on an HP 1100 HPLC, was employed to calculate number average molecular weight, weight average molecular weight, and polydispersity. PL gel MIXED-C 300 - 7.5 mm column (packed with 5 micron particles of different pore sizes) allowed the separation of polymers over a wide molecular weight (range of 200-3,000,000). All samples were dissolved in tetrahydrofuran (THF) and were then

introduced into the solvent stream going through the column. HP 1047A refractive index detector monitors the concentration of sample exiting the end of the column. THF was used as the eluent at a flow rate of 1 mL/min at 35 °C.

F. Fourier Transform Infrared (FTIR)

FTIR was used to examine the chemical composition of the synthesized polymers. FTIR spectra were recorded by Perkin Elmer SpectrumOne® FTIR spectrometer by using potassium bromide (KBr) disk as a background. The polymeric nanocomposites were mixed with the dried KBr powder and pressed into a translucent thin disk for the scan. All the samples undergo 25 scans from 4000 to 400 wavenumbers, and an average spectrum was obtained.

CHAPTER 4

RESULTS AND DISCUSSIONS

The present chapter is divided into six sections. Section 4.1 presents the general characterization of PMMA/silica nanocomposites synthesized in supercritical carbon dioxide. Section 4.2 presents the characterization of PMMA/silica nanocomposites synthesized in supercritical carbon dioxide with various surfactant concentrations. Section 4.3 presents the characterization of PMMA/silica nanocomposites synthesized in supercritical carbon dioxide with various filler concentrations. Section 4.4 presents the monolith of PMMA/silica nanocomposites synthesized in supercritical carbon dioxide. Section 4.5 presents the thermal stability and mechanical properties of PMMA/silica nanocomposites synthesized in supercritical carbon dioxide and their comparisons with melt mixing nanocomposites. Section 4.6 presents the characterization of PMMA/iron oxide nanocomposite monoliths synthesized in supercritical carbon dioxide. In this study, the characterization methods include:

1) Surface morphology of the nanocomposites by SEM.

2) Examination of the chemical composites Fourier transform infrared analysis (FTIR).

3) Examination of the thermal stability by thermogravimetric analysis (TGA).

4) Examination of the glass transition temperature by differential scanning calorimetry analysis (DSC).

4.1 General Characterization of PMMA/Silica Nanocomposites Synthesized in Supercritical Carbon Dioxide

4.1.1 Synthesis of Silica Particles and Surface Functionalization

Silica nano-particles were synthesized according to the process described by Stober et al. (1968). In the process, TEOS was hydrolyzed to form silica particles in ethanol with NH_4OH catalyst at room temperature. Monodisperse spherical silica particles of controlled sizes could be synthesized by changing the concentrations of reactant and catalyst. In the synthesis, TEOS (46.8 ml) were hydrolyzed to form silica particles in ethanol (300 ml) with the catalyst, NH_4OH (28.2 ml), at room temperature over a period of two days. As show in Figure 4.1 (a), the SEM micrograph of silica particles have an average diameter of 75 nm. The slight irregular particle surfaces as shown in Figure 4.1 (b) originate from the layer of the coupling agent MPS. Though slight agglomeration is observed in the micrograph, we observed that MPS-modified silica dispersed very well in supercritical carbon dioxide even without stirring. This is probably due to the favorable interactions between MPS molecules and carbon dioxide. Earlier studies showed that silica particles can be stabilized by PDMS in supercritical carbon dioxide (Calvo et al., 2000; Christain et al., 2000; Sirard et al., 2004). In a different study, silica nano-particles modified with fluorinated chlorosilanes was found to disperse well in supercritical carbon dioxide (Yates et al., 2000). In this work, we found successful dispersion of MPS-modified silica nano-particles in supercritical carbon dioxide, in agreement with the work by Yue et al. (2005).

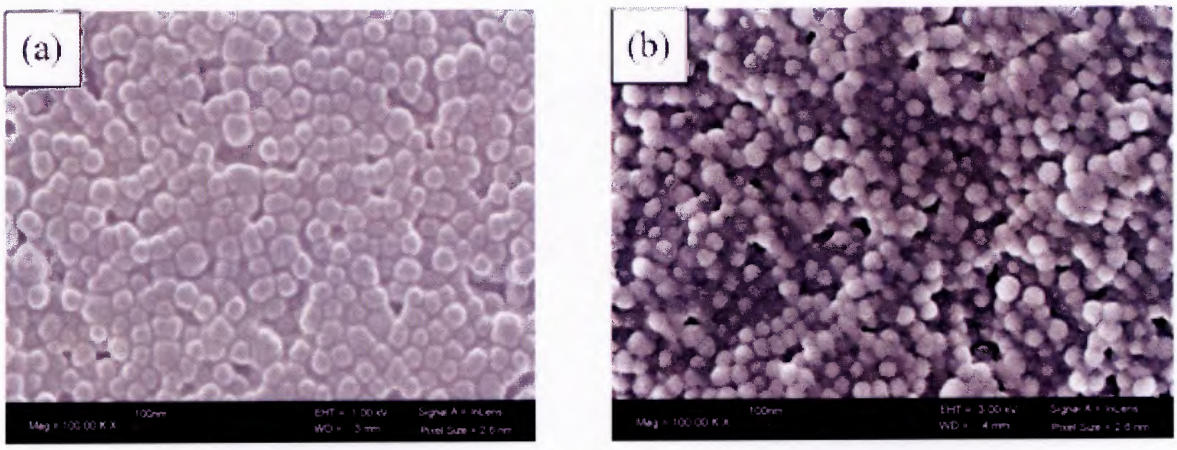

Figure 4.1 SEM images of (a) silica particles (b) surface modified silica particles with average size of 75 nm

4.1.2 Synthesis of PMMA/Silica Nanocomposites

Figure 4.2 depicts SEM micrograph of the nanocomposites prepared from PMMA with 10wt. % 75nm silica nano-particles. The micron-sized polymeric nanocomposites formed an interconnected macroporous structure which filled up uniformly the entire reactor. Small encapsulated silica nano-particles can be seen from the surface morphology of the nanocomposites; no bare silica particle was found excluded from the PMMA matrix. The pore size distribution was in a range of few microns.

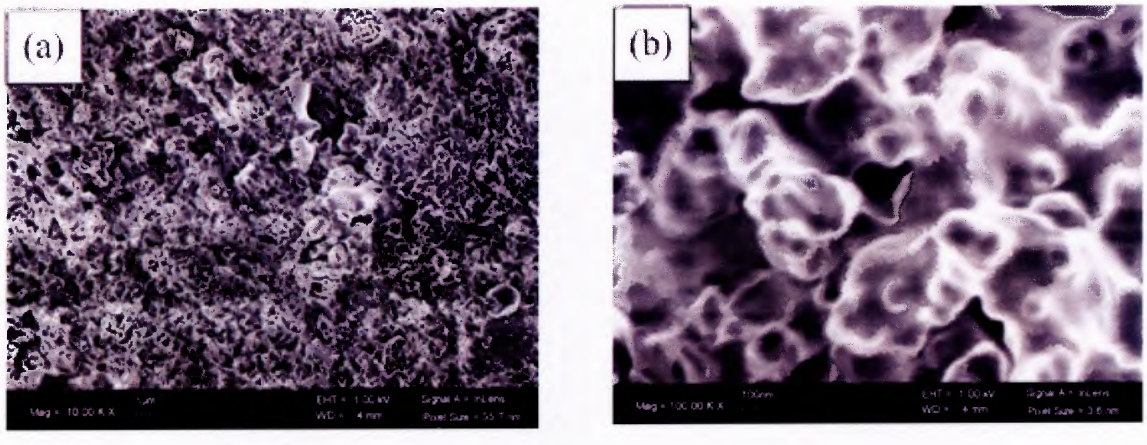

Figure 4.2 SEM images of (a) and (b) PMMA/silica nanocomposites containing the surface modified silica nano-particles prepared via dispersion polymerization in supercritical carbon dioxide. Image of (b) is the magnification of (a).

In this work, the progress of the reaction was monitored visually through the sapphire windows on the two sides of the reactor. Initially, the reaction medium was transparent with observable traces of strong convective motions. Approximately two hours after the reaction temperature and pressure were reached, the turbidity of the medium started to increase gradually. After four hours, no light could penetrate through the reaction medium and a milky-white appearance similar to conventional aqueous latex was observed in the area close to the windows. However, no precipitation was observed until a few more hours later.

4.1.3 Fourier Transform Infrared (FTIR) Analysis

In this study, samples were mixed with KBr pellets and then pressed for FTIR measurement to identify the composition of the samples. Figure 4.3 shows the IR spectra of (a) the bare synthesized silica particles, (b) the surface modified silica particles, (c) PMMA/silica nanocomposites without surfactant PDMS-MA, and (d) PMMA/silica nanocomposites synthesized with surfactant PDMS-MA.

From curve (a), the -OH stretching peak at 3000~3600 cm^{-1}, the Si-OH stretching peak at 960 cm^{-1}, and the stretching of Si-O-Si peaks at 460 cm^{-1}, 800 cm^{-1}, and 1100~1250 cm^{-1} were found. It was also found that tetraethyl orthosilicate (TEOS) was hydrolyzed completely to form silica particles with hydrophilic surface; the $-C_2H_5$ stretching peak was not observed in the spectrum.

From curve (b), the peaks at 460 cm^{-1}, 800 cm^{-1}, and 1100~1250 cm^{-1}, show that the presence of silica particles. The C-O stretching peak at 1247 cm^{-1}, the C=C stretching peak at 1640 cm^{-1}, the C=O stretching peak at 1730 cm^{-1}, and the C-H stretching peak at 2927 cm^{-1} show that after the attachment of MPS, MPS reacted with the hydroxide groups and turned the silica surface from hydrophilic into hydrophobic with methacrylate terminal groups. This

proves a successful reaction between MPS and the surface of hydrophilic silica particles. The position of the -OH stretching peak at 3000~3600 cm^{-1}, implicating the formation of hydrogen bonding, reveals that the hydrophilic surface of silica nano-particles could not be completely modified by MPS.

From curve (c), the Si-O-Si stretching peaks at 460 cm^{-1}, 800 cm^{-1}, and 1100~1250 cm^{-1} show the presence of silica particles. The peak at 1247 cm^{-1} assigned to the C-O stretching, the peak at 1730 cm^{-1} assigned to the C=O stretching, and the peak at 2927 cm^{-1} assigned to the C-H stretching indicate the presence of synthesized PMMA.

From curve (d), the Si-O-Si stretching peaks at 460 cm^{-1}, 800 cm^{-1}, and 1100~1250 cm^{-1} also show the presence of silica particles. The C-O stretching peak at 1247 cm^{-1}, the C=O stretching peak at 1730 cm^{-1}, and the C-H stretching peak at 2927 cm^{-1} indicate the presence of synthesized PMMA. The Si-C stretching peak at 1259 cm^{-1} indicate the presence of the surfactant PDMS-MA. Note that the -MA group of this surfactant allows it to react with MMA and with the growing PMMA chains.

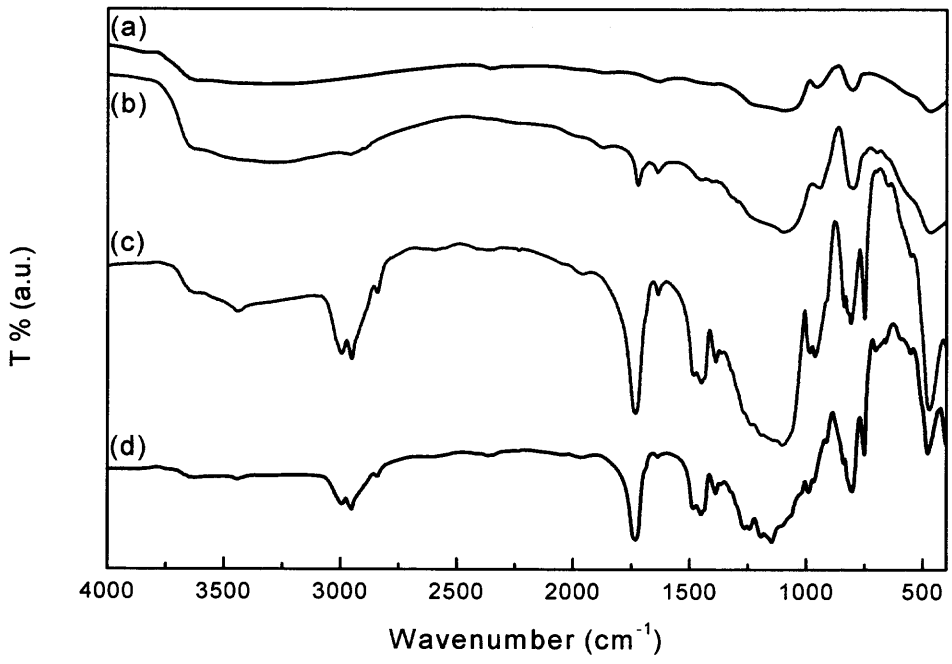

Figure 4.3 FTIR spectra of (a) synthesized silica; (b) synthesized surface modified silica; (c) PMMA/surface modified silica composites without surfactant PDMS-MA; (d) PMMA/surface modified silica composites with surfactant PDMS-MA.

In summary, the silica nano-particles with an average diameter of 75 nm were synthesized and were successfully functionalized by MPS via the reaction with the hydroxide groups on the silica surface. The functionalization also turned the silica surface from hydrophilic into hydrophobic and made the particles suspended well in ScCO2. The functionalization and the in-situ grafting of PMMA chains on the silica surface were verified by the FTIR spectra and SEM micrographs.

4.2 Synthesis of PMMA/Silica Nanocomposites in Supercritical Carbon Dioxide with various Surfactant Concentrations

4.2.1 Surface Morphology

A major technological barrier for achieving superior properties of nano-structured composite materials is the difficulty of dispersing fillers uniformly in a host matrix. One of the promising nanocomposite manufacture processes to achieve property improvements is through chemical modifications of filler structures and utilization of chemical interactions between the chemically modified fillers and the matrix polymers. We have developed a novel and efficient supercritical fluid processing method for surface modified nano-scale fillers for the use in polymeric nanocomposites. The surface morphology of the nanocomposites synthesized in the supercritical carbon dioxide can be controlled by changing process parameters.

Surfactant stabilizer plays a vital role in dispersion polymerization. It has been reported that the yield of polymerizations is lower in an un-stabilized system than in a stabilized system. Increasing the surfactant concentration results in a smaller average of dispersed polymer particles and an increase of particle number density (Christian et al. 2000). In this study, poly (dimethylsiloxane) methacrylate (PDMS-MA) was employed as surfactant stabilizer. In each run, 2 ml of monomer MMA, 0.04 g of initiator AIBN, 0.2 g of silica nano-particles, and various concentration of PDMS-MA were premixed followed by purging with low-pressure carbon dioxide for five minutes, liquefied carbon dioxide was pumped into the reactor at room temperature until an appropriate pressure was reached. Figure 4.4 depicts the surface morphology of PMMA/silica nanocomposites with four PDMS-MMA/MMA volume ratios: (a) and (b) 0 vol. % ; (c) and (d) 5 vol. %; (e) and (f) 10 vol. %; (g) and (h) 20 vol. %. The reaction conditions were set constant as T= 65°C and P=27580 MPa during the 24-hour run.

Figure 4.4 (a) and (b) show that if there was no surfactant, PMMA cannot be coated on silica nano-particles and the bare nano-particles were scattered around the agglomerated PMMA particles which had irregular shapes and smooth surfaces. As the surfactant concentration was raised to 5 vol. %, Figure 4.4 (c) and (d) depict a rougher surface morphology of the nanocomposite compared to the case of no surfactant; the observed SEM micrographs suggest the encapsulation of the nano-particles inside the PMMA particles. The PMMA composite particles also exhibited a less degree of agglomeration and were more spherical compared to the case of 0% surfactant. There are still some scattered silica particles which were not included in the composites; however, the amount is much smaller.

As the surfactant concentration increases to 10 vol. %, discrete composites particles with a narrow size distribution around 1-2 μm are observed in Figure 4-4 (e) and (f). The shape of the composite particles is roughly spherical, while the surface morphology shows the inclusion of nano-particles around the surface. Compared to Figure 4.4 (d), Figure 4.4 (f) shows no bare silica nano-particle scattered around the sample. The increase of the surfactant facilitates the inclusion and dispersion of the nano-particles in the composites and the morphology of the polymeric composite becomes more discrete.

In Figures 4.4 (g) and (h), rough morphology of PMMA/silica nanocomposite particles with a relative wide size distribution was observed for the case of the surfactant concentration equal to 20 vol. %. The rough morphology could attribute to the excessive polymer particles stabilized by the surfactants, which reduces the degree of coalescence and combination of polymer-grafted nano-particles during the process of polymerization. In general, the scanning electron microscopy micrographs show that higher surfactant concentration results in higher number density of polymeric nanocomposite particles and better dispersion of the

nano-particles in the composites. This observation reveals the importance of stabilization during nucleation and growth of polymer domains on the surface of the silica nano-particles.

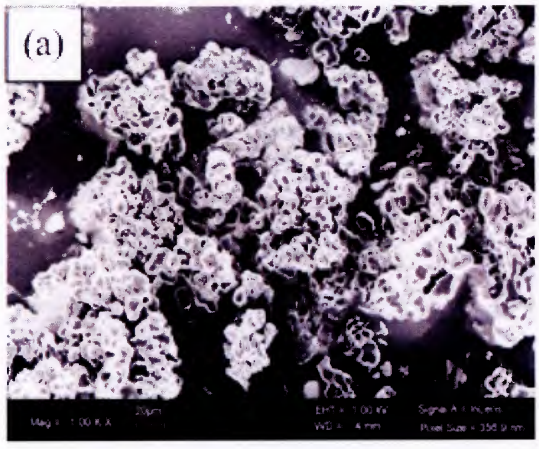

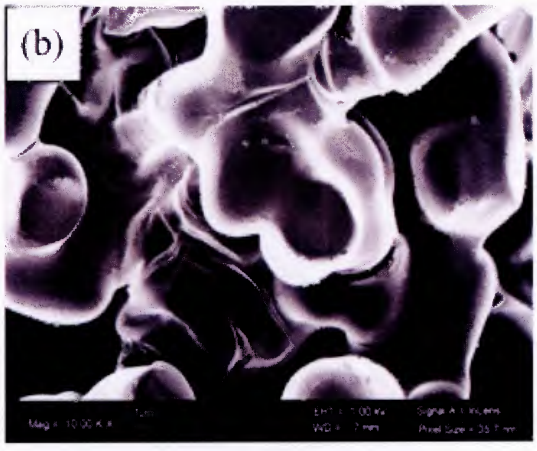

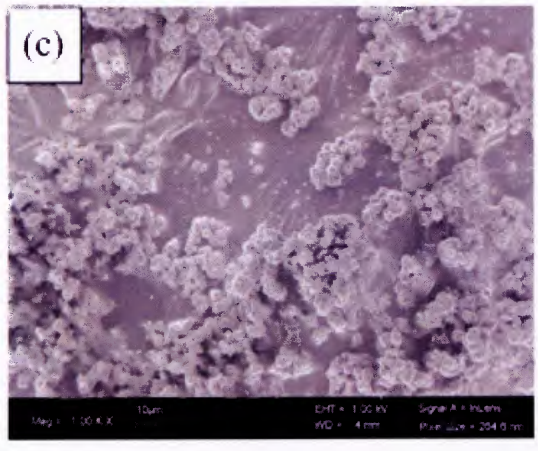

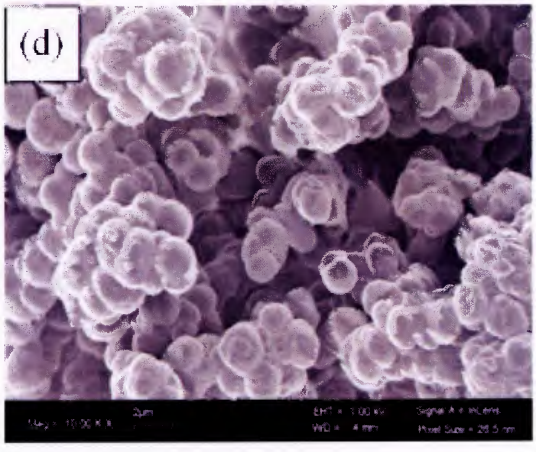

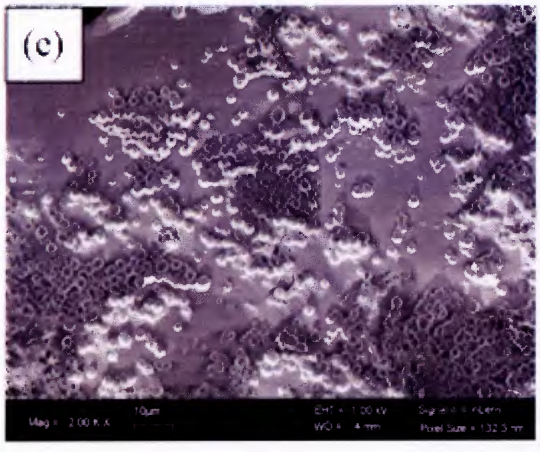

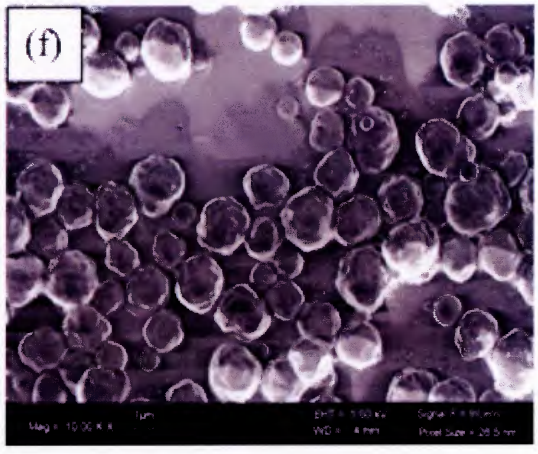

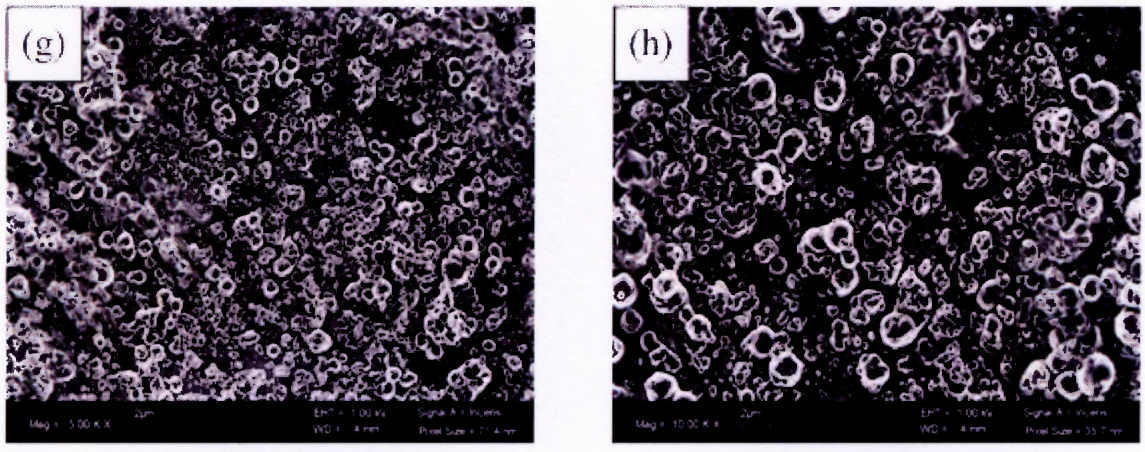

Figure 4.4 SEM images of (a) PMMA/silica nanocomposite containing no surfactant, (b) the magnification of (a); (c) PMMA/silica nanocomposites containing 5 vol. % surfactant, (d) the magnification of (c); (e) PMMA/silica nanocomposites containing 10 vol. % surfactant, (f) the magnification of (e); (g) PMMA/silica nanocomposites containing 20 vol. % surfactant, (h) the magnification of (g). The concentration of silica particle in the synthesis is 10 wt. % in all specimens.

4.2.2 Thermogravimetric Analysis (TGA)

Thermogravimetric analysis is performed on weight changes of the smaples in relation to the change in temperature. This analysis relies upon a high degree of precision in three measurements: weight, temperature, and temperature change. It is commonly employed to determine the characteristics, the degradation temperature, the absorbed moisture content of materials, the ratio of inorganic and organic components, and the decomposition points of the samples.

Figure 4.5 depicts the TGA results of the weight loss percentage (%) versus temperature (^{o}C) of the samples: (a) PMMA/silica nanocomposite containing 0 vol. % surfactant; (b) PMMA/silica nanocomposites containing 5 vol. % surfactant; (c) PMMA/silica nanocomposites containing 10 vol. % surfactant; and (d) PMMA/silica nanocomposites containing 20 vol. % surfactant. All specimens were prepared with 10 wt. % silica particles in the synthesis.

The weight loss profile of TGA could be roughly divided into three stages. The first stage, denoting the temperature range between 25–170°C with a weight loss of about 3%, is attributed to the loss of water and low boiling point organic residues. The second stage, a significant weight loss in the range of 170–400°C in each of (a), (b), (c), and (d) is attributed to the decomposition of PMMA where PMMA decomposes in two sections: in the first section, the weight loss gradually decreases as it is loaded with various organic silica composite. The degradation of PMMA is related to the interaction between the radical-polymerized PMMA. In the second section, the degradation of PMMA is attributed to the presence of head-to-head linkages, the lack of saturation of the end groups related to the combination and termination of two radicals and random scission (Chang et al., 2000).

The third stage, featuring no weight loss between 400 and 500°C, is related to the presence of 10% silica nano-particles. Quantitatively, the heat decomposition temperature (Td), defined as the temperature at 10% weight losses, increases from (a) 181°C, (b) 182°C, (c) 239°C to (d) 243°C. This is attributed to the effect of surfactant: increasing surfactant concentration results in higher average molecular weight during the polymerization. This argument is supported by the results from gel permeation chromatography. As shown in Figure 4.6 and Table 4.1, the molecular weight increases from (a) 85027, (b) 122515, (c) 157985, to (d) 190988.

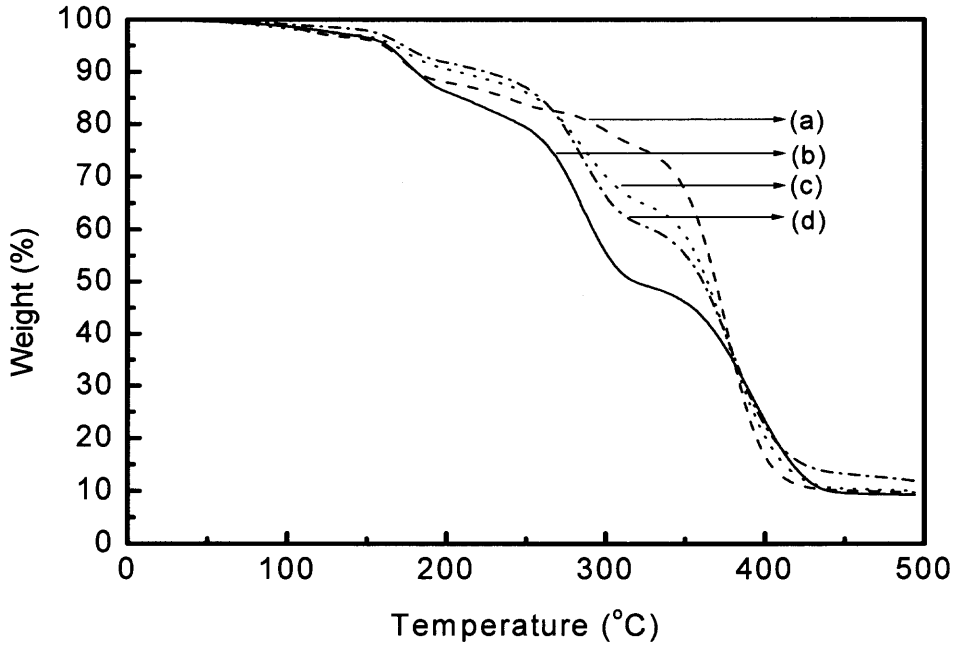

Figure 4.5 Weight percentage vs. temperature plots obtained from TGA (10°C/min) of (a) PMMA/silica nanocomposite containing 10 % silica synthesized with 0 vol. % surfactant; (b) PMMA/silica nanocomposites containing 10 wt. % silica synthesized with 5 vol. % surfactant; (c) PMMA/silica nanocomposites containing 10 wt. % silica synthesized with 10 vol. % surfactant; (d) PMMA/silica nanocomposites containing 10 wt. % silica synthesized with 20 vol. % surfactant.

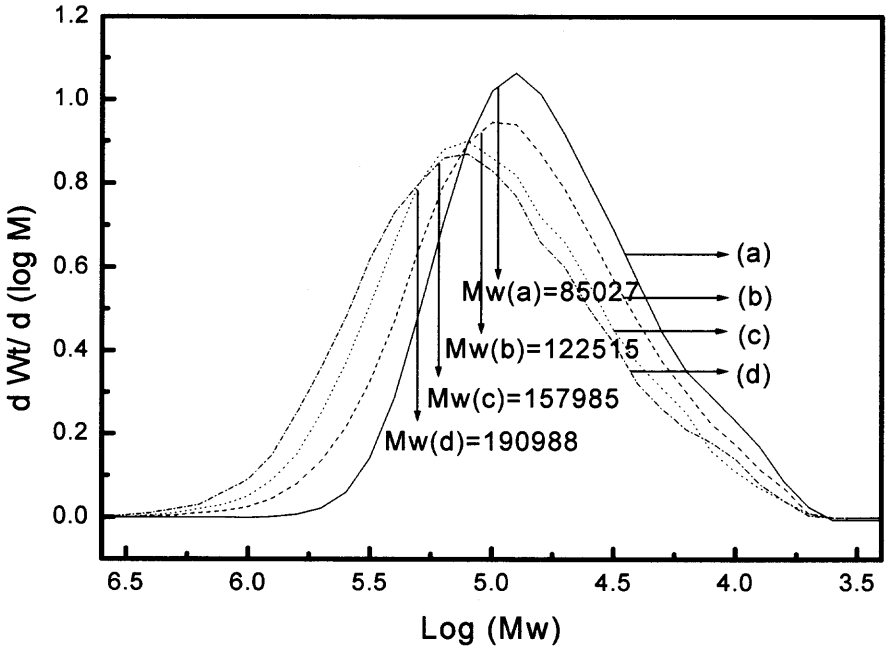

Figure 4.6 Molecular weight distribution obtained from GPC of (a) PMMA/silica nanocomposite containing 10 % silica synthesized with 0 vol. % surfactant; (b) PMMA/silica nanocomposites containing 10 wt. % silica synthesized with 5 vol. % surfactant; (c) PMMA/silica nanocomposites containing 10 wt. % silica synthesized with 10 vol. % surfactant; (d) PMMA/silica nanocomposites containing 10 wt. % silica synthesized with 20 vol. % surfactant.

Table 4.1 Results of GPC

Sample	Mn	Mw	Polydispersity
(a)	40973	85027	2.1
(b)	41746	122515	3.0
(c)	51602	157985	3.1
(d)	61203	190988	3.2

4.2.3 Differential Scanning Calorimetry (DSC) Analysis

In this study, DSC was employed to test the heat flow rates and glass transition temperatures of the four samples: (a) PMMA/silica nanocomposite containing 10 % silica synthesized with 0 vol. % surfactant; (b) PMMA/silica nanocomposites containing 10 wt. % silica synthesized with 5 vol. % surfactant; (c) PMMA/silica nanocomposites containing 10 wt. % silica synthesized with 10 vol. % surfactant; and (d) PMMA/silica nanocomposites containing 10 wt. % silica synthesized with 20 vol. % surfactant.

Fig. 4.7 and Fig. 4.8 show the DSC thermograms of the samples during 1st cooling and 2nd heating cycles, respectively. From the cooling procedure, the glass transition temperature of (a) is 117.23°C, which changes to 118.71°C in (b), to 121.59°C in (c), and to 122.54°C in (d). From the 2nd heating procedure, the glass transition temperature is 119.21°C in (a), 120.33°C in (b), 121.42°C in (c) and 123.75°C in (d); the glass transition temperature increases slightly from (a), (b), (c), to (d). The heat flow rates increase from (a), (b), (c), to (d) during the cooling procedure; a similar result was observed during the heating procedure. The DSC results have shown, to a noticeable extent, how the presence of the surfactant, PDMS-MA, affects the mobility of polymer chains, and the increasing surfactant concentration results in higher polymer molecular weight, and thus the glass transition temperature. Thermal stability can be improved in certain applications with higher glass transition temperature.

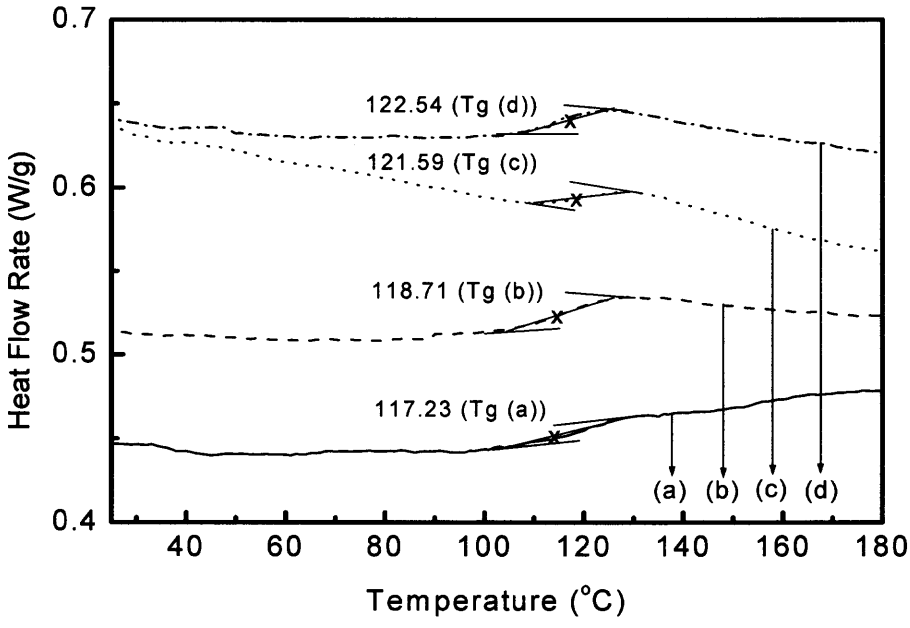

Figure 4.7 DSC results of the 1st cooling cycle (10°C/min) of (a) PMMA/silica nanocomposite containing 10 % silica synthesized with 0 vol. % surfactant; (b) PMMA/silica nanocomposites containing 10 wt. % silica synthesized with 5 vol. % surfactant; (c) PMMA/silica nanocomposites containing 10 wt. % silica synthesized with 10 vol. % surfactant; (d) PMMA/silica nanocomposites containing 10 wt. % silica synthesized with 20 vol. % surfactant.

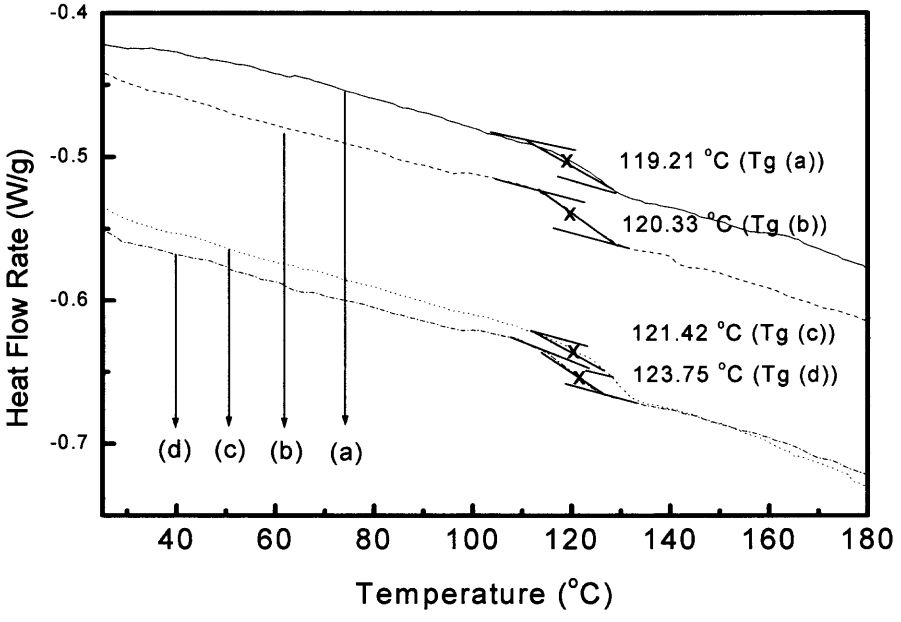

Figure 4.8 DSC results of the 2nd heating cycle (10°C/min) of (a) PMMA/silica nanocomposite containing 10 % silica synthesized with 0 vol. % surfactant; (b) PMMA/silica nanocomposites containing 10 wt. % silica synthesized with 5 vol. % surfactant; (c) PMMA/silica nanocomposites containing 10 wt. % silica synthesized with 10 vol. % surfactant; (d) PMMA/silica nanocomposites containing 10 wt. % silica synthesized with 20 vol. % surfactant.

Table 4.2 Glass transition temperature obtained from DSC for samples synthesized with various surfactant concentrations

Sample	1st Cooling Temperature (°C)	2nd Heating Temperature (°C)
(a)	117.23	119.21
(b)	118.71	120.33
(c)	121.59	121.42
(d)	122.54	123.75

4.3 Synthesis of PMMA/Silica Nanocomposites in Supercritical Carbon Dioxide with various Filler Concentrations

4.3.1 Surface Morphology

In this subsection, the effect of the filler concentration on the surface morphology of PMMA/silica nanocomposites was studied by scanning electron microscopy. The reactions were conducted at four different functionalized silica (g) /MMA (ml) ratios: 0 %, 5 %, 10 %, and 20 %. The ratio of the surfactant to the filler was kept constant as 1ml PDMS-MA to 1 g functionalized silica. Therefore, the corresponding surfactant concentrations (PDMS-MA (ml) /MMA (ml)) are 0 %, 5 %, 10 %, and 20 %, respectively. The concentration of the initiator is 2 % and the reaction was conducted in the high pressure reactor at 65°C and 27580 MPa for 24 hours. When the silica (g)/MMA (ml) ratio was 0 wt. % , profound coagulation of PMMA with very irregular shapes and some pores caused by depression of the $ScCO_2$ was observed in Figure 4.9 (a) and (b). Increasing the silica (g)/ MMA (ml) ratio to 5 wt. %, as shown in Figure 4.9 (c) and (d), discrete or loosely agglomerated composite particles from 2 to 4 μm in diameters were observed. The particles had narrow size distribution and uneven surface morphology showing the inclusion of the nano-particles. When the silica (g)/MMA (ml) ratio was increased to 10 wt. %, as shown in Figure 4.9 (e) and (f), all the composite particles are discrete and the size reduced to be around 1-2 μm in diameters. The size distribution was narrow and surface morphology remained uneven showing the inclusion of nano-particles. Increasing the silica (g)/MMA (ml) ratio to 20 wt. %, as shown in Figure 4.9 (g) and (h), the composite particles turned to be around 200nm and formed an interconnected porous structure which extended uniformly into the entire space of the mold. The size of the pores was in the range of submicron and the synthesized nanocomposites exhibited a macroporous monolith.

The increase of the filler and surfactant concentrations showed a drastic change of the morphology of the nanocomposites from discrete particles to an interconnected macroporous structure.

The amount of silica nano-particles can affect the product morphology. Higher contents of silica nano-particles in the composites cause more nucleation sites for the precipitation of the polymer molecules and more reaction sites for dispersion polymerization.

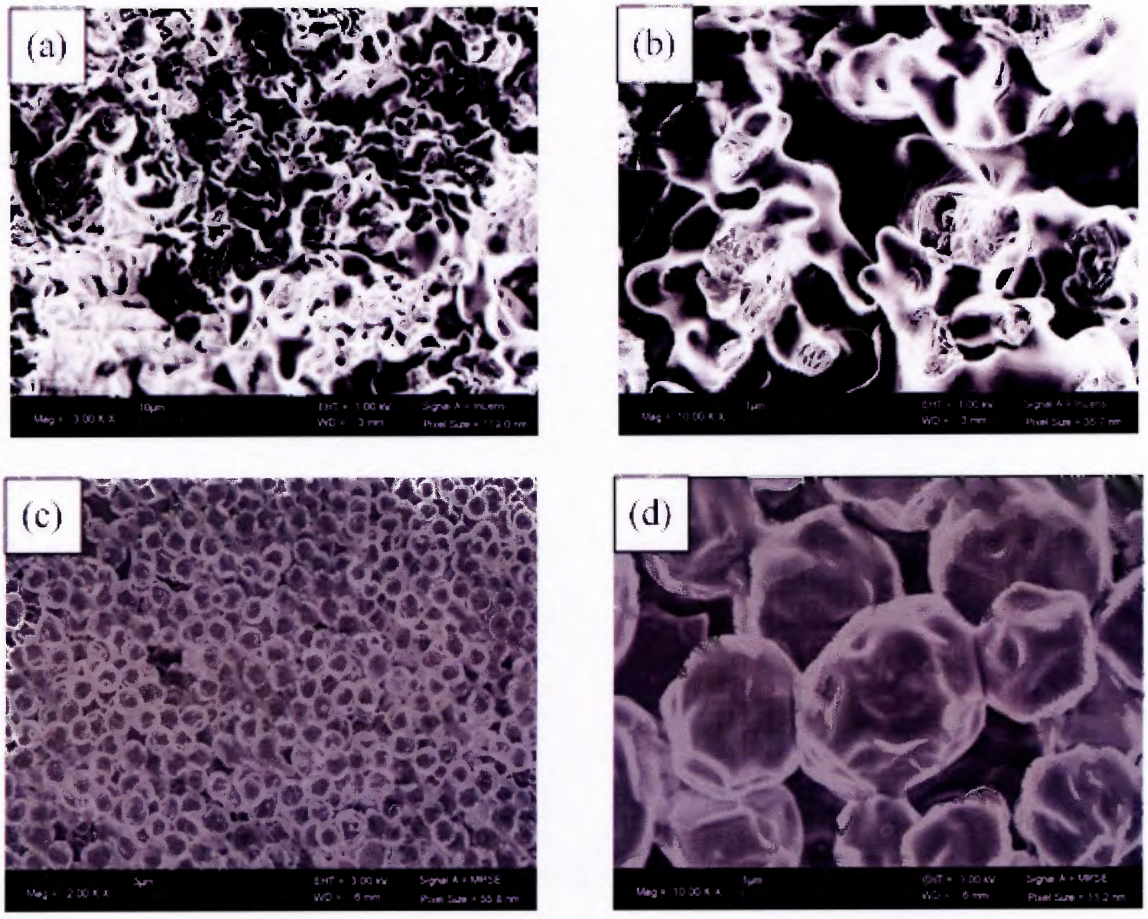

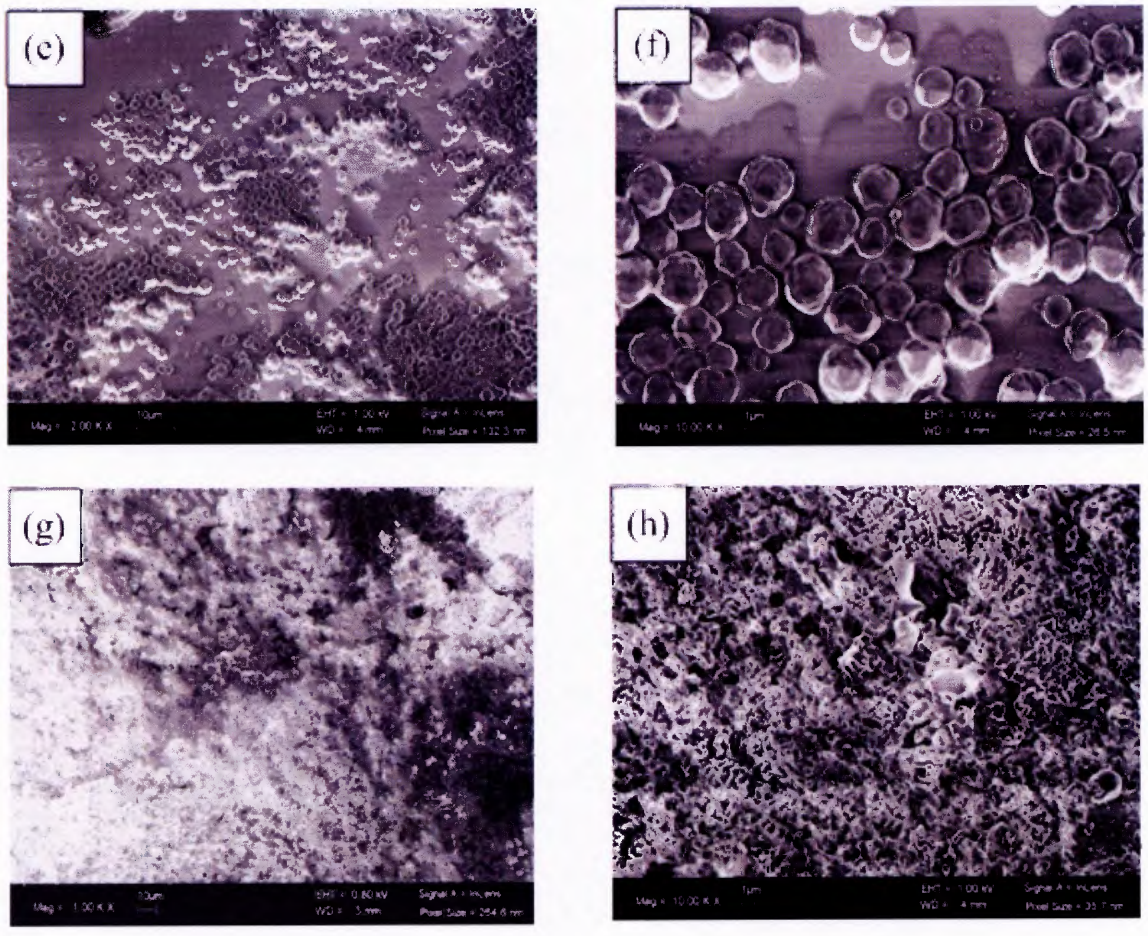

Figure 4.9 SEM images of (a) (b) synthesized pure PMMA containing 0 wt. % silica synthesized with 0 vol. % surfactant, image of (b) is the magnification of (a); (c) (d) PMMA/silica nanocomposites containing 5 wt. % silica synthesized with 5 vol. % surfactant, image of (d) is the magnification of (c); (e) (f) PMMA/silica nanocomposites containing 10 wt. % silica synthesized with 10 vol. % surfactant, image of (f) is the magnification of (e); (g) (h) PMMA/silica nanocomposites containing 20 wt. % silica synthesized with 20 vol. % surfactant, image of (h) is the magnification of (g).

To single out the effect of surfactant concentration, comparison of the same surfactant concentration 20 vol. % was made in Figure 4.10. All the rest reaction conditions were kept constant. The filler concentration was made to change from 0 wt. %, Figure 4-10 (a) and (b); 10 wt. %, Figure 4-10 (c) and (d); to 20 wt. %, Figure 4-10 (e) and (f).

As shown in Figure 4.10 (a) and (b) of 0 wt. % filler, agglomeration of spheric PMMA particles of 1 micron in diameters together with heavily agglomerated smaller particles were

observed. An excessive amount of surfactant may lead to the observed agglomeration during the depressurization process due to the low glass transition temperature (-59°C) of the surface PDMS which enhances the fusion and agglomeration of the particles. Increasing the filler concentration to 10 wt. %, Figure 4-10 (c) and (d) display clearly a bimodal distribution of the particle size: some large composite particles with a size around 1 μm were found scattered among the agglomerated particles of sizes around 100-200 nm. The composite materials again formed a macroporous monolith when removed from the reactor. Increasing the silica (g)/MMA (ml) ratio to 20 wt. %, as shown in Figure 4.10 (e) and (f), the micron-sized polymeric nanocomposite particles disappear; the prevalent small particles (~200nm) aggregated and formed an interconnected macroporous structure which extended uniformly into the entire space of the mold. The disappearance of the large particles implicated that the number density of the dispersed polymer colloids formed via spontaneous nucleation (i.e. without the participation of the silica nano-particles) decreased drastically upon the increase of the filler concentration, which enhance the nucleation sites for the precipitation of polymer followed by agglomeration to form macroporous monolith.

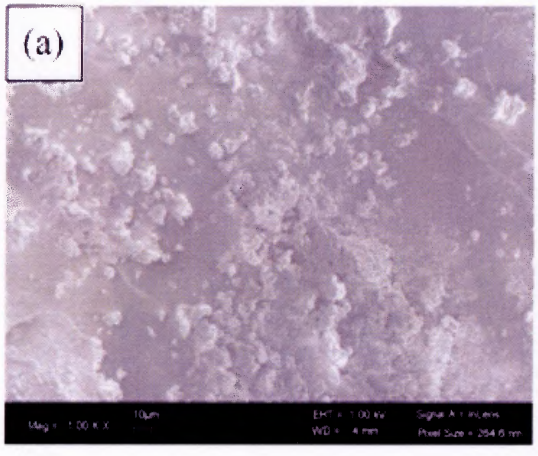

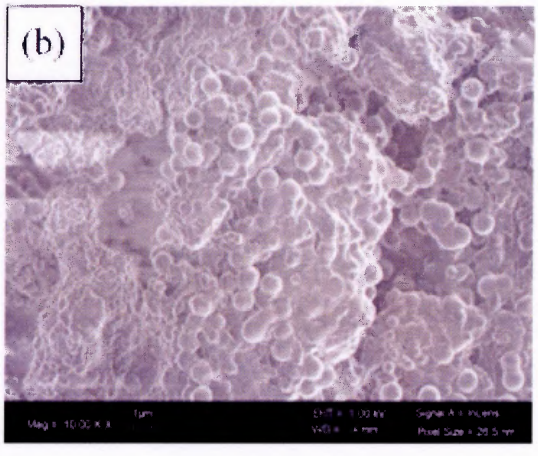

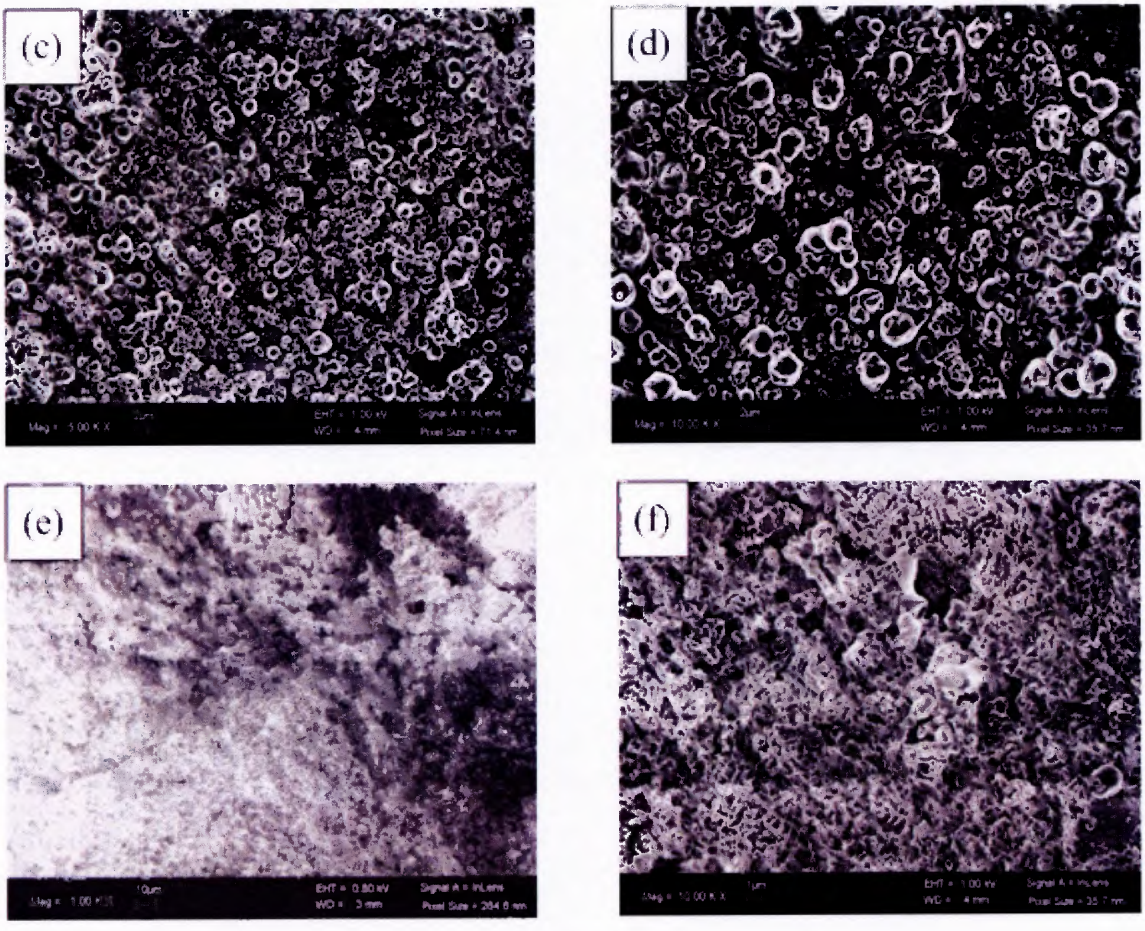

Figure 4.10 SEM images of (a) (b) synthesized PMMA containing 0 wt. % silica synthesized with 20 vol. % surfactant, image of (b) is the magnification of (a); (c) (d) synthesized PMMA containing 10 wt. % silica synthesized with 20 vol. % surfactant, image of (d) is the magnification of (c); (e) (f) synthesized PMMA containing 20 wt. % silica synthesized with 20 vol. % surfactant, image of (f) is the magnification of (e).

4.3.2 Thermogravimetric Analysis (TGA)

Thermogravimetric analysis can be employed to determine the characteristics, the degradation temperatures, the absorbed moisture content, the ratio of inorganic and organic components in materials, and the decomposition point. One important feature of nanocomposite is the enhancement of certain physical properties due to the addition of nano-fillers, especially the thermal properties.

Figure 4.11 depicts the TGA results of weight loss percentage (%) versus temperature (^{o}C) of the samples: (a) PMMA/silica nanocomposite containing 0 wt. % silica synthesized with 0 vol. % surfactant; (b) PMMA/silica nanocomposites containing 5 wt. % silica synthesized with 5 vol. % surfactant; (c) PMMA/silica nanocomposites containing 10 wt. % silica synthesized with 10 vol. % surfactant; and (d) PMMA/silica nanocomposites containing 20 wt. % silica synthesized with 20 vol. % surfactant.

The weight loss profile in TGA could be roughly divided into three stages. The first stage, denoting the temperature range between 25–170°C with a weight loss of about 3%, is attributed to the loss of water and low boiling point organic residues. The second stage, a significant weight loss in the range of 170–400°C for all curves is attributed to the decomposition of PMMA. The third stage, featuring no weight loss between 400 and 500°C, is related to the presence of silica nano-particles. Calculations from the TGA data yielded the real silica nano-particle weight percentage in these four samples are respectively 0 %, 5 %, 11 %, and 22%. These data are comparable to the added filler amount of 0 %, 5 %, 10 %, and 20%. Quantitatively, the heat decomposition temperature (T_d), defined as the temperature at 10% weight loss, increases from (a) 235^{o}C, (b) 237^{o}C, (c) 239^{o}C to (d) 254^{o}C. In comparison to the PMMA homopolymer, silica nano-particles enhanced the thermal stability of PMMA but only slightly.

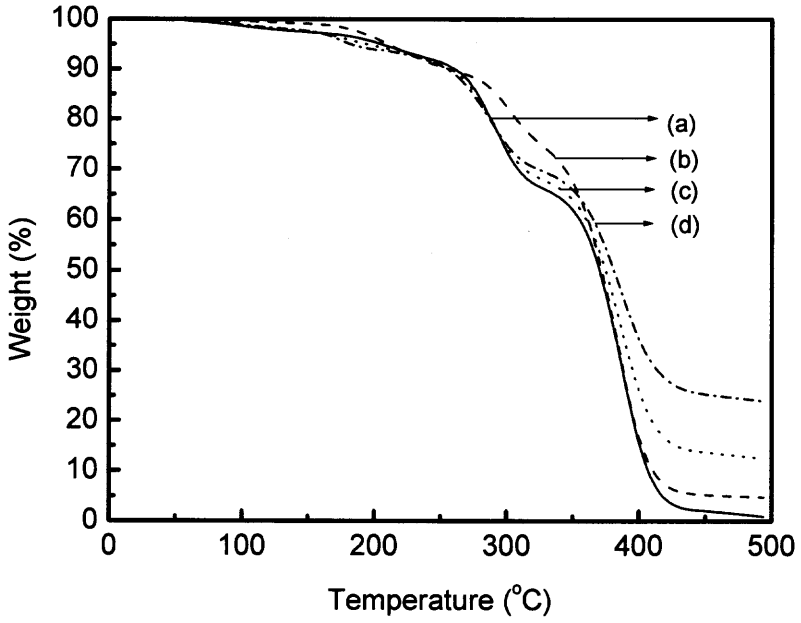

Figure 4.11 TGA results of weight percentage vs. temperature of (a) PMMA/silica nanocomposite containing 0 % silica synthesized with 0 vol. % surfactant; (b) PMMA/silica nanocomposites containing 5 wt. % silica synthesized with 5 vol. % surfactant; (c) PMMA/silica nanocomposites containing 10 wt. % silica synthesized with 10 vol. % surfactant; (d) PMMA/silica nanocomposites containing 20 wt. % silica synthesized with 20 vol. % surfactant.

4.3.3 Differential Scanning Calorimetry Analysis (DSC)

In this subsection, DSC was employed to test the heat flow rates and glass transition temperatures of the four samples samples: (a) PMMA/silica nanocomposite containing 0 wt. % silica synthesized with 0 vol. % surfactant; (b) PMMA/silica nanocomposites containing 5 wt. % silica synthesized with 5 vol. % surfactant; (c) PMMA/silica nanocomposites containing 10 wt. % silica synthesized with 10 vol. % surfactant; and (d) PMMA/silica nanocomposites containing 20 wt. % silica synthesized with 20 vol. % surfactant.

From the cooling procedure, the glass transition temperature changes from 110.76°C in (a), to 115.43°C in (b), 116.13°C in (c), and 122.83°C in (d). From the 2nd heating procedure, the

glass transition temperature is 114.17°C in (a), 117.46°C in (b), 118.76°C in (c) and 125.31°C in (d); the glass transition temperature increases slightly from (a), (b), (c), to (d). The heat flow rates increase from (a), (b), (c), to (d) during the cooling procedure; a similar result was observed during the heating procedure. The DSC results have shown, to a noticeable extent, how the filler concentration affects the mobility of polymer chains, and thus the glass transition temperature. Since the presence of nanoparticles will hinder the polymer mobility, the glass transiton temperature is usually higher than neat polymer, unless cavities form around the nanoparticles during processing or synthesis. Thermal stability in certain applications can be improved with higher glass transition temperature.

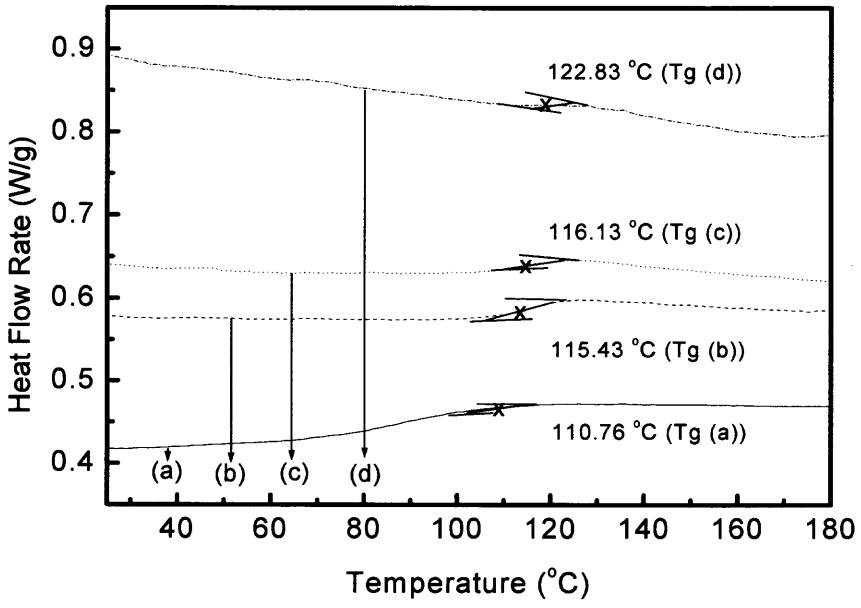

Figure 4.12 DSC results of the 1st cooling cycle (10°C/min) of (a) PMMA/silica nanocomposite containing 0 % silica synthesized with 0 vol. % surfactant; (b) PMMA/silica nanocomposites containing 5 wt. % silica synthesized with 5 vol. % surfactant; (c) PMMA/silica nanocomposites containing 10 wt. % silica synthesized with 10 vol. % surfactant; (d) PMMA/silica nanocomposites containing 20 wt. % silica synthesized with 20 vol. % surfactant.

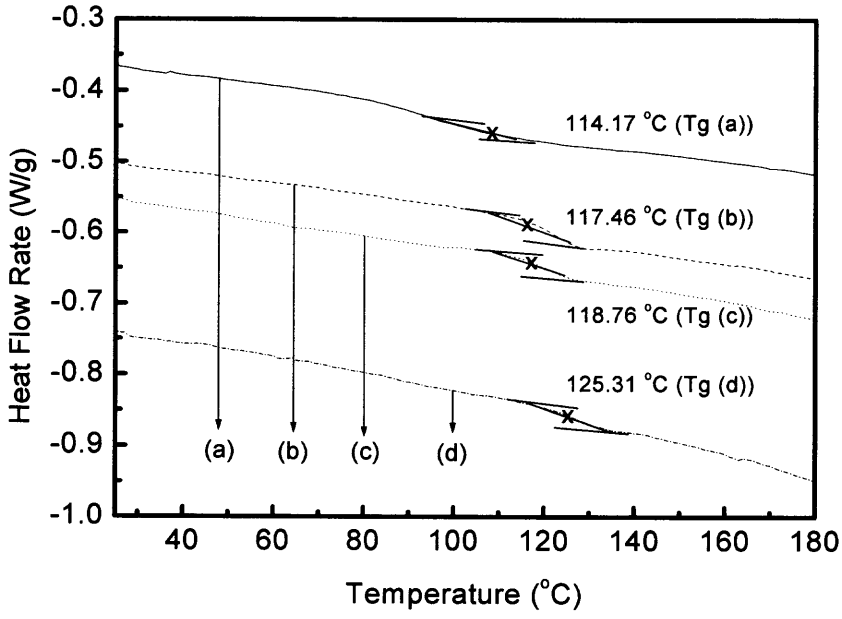

Figure 4.13 DSC results of the 2nd heating cycle (10°C/min) of (a) PMMA/silica nanocomposite containing 0 % silica synthesized with 0 vol. % surfactant; (b) PMMA/silica nanocomposites containing 5 wt. % silica synthesized with 5 vol. % surfactant; (c) PMMA/silica nanocomposites containing 10 wt. % silica synthesized with 10 vol. % surfactant; (d) PMMA/silica nanocomposites containing 20 wt. % silica synthesized with 20 vol. % surfactant.

Table 4.3 Glass transition temperature obtained from DSC for samples synthesized with various filler concentrations

Sample	1st Cooling Temperature (°C)	2nd Heating Temperature (°C)
(a)	110.76	114.71
(b)	115.43	117.46
(c)	116.13	118.76
(d)	122.83	125.31

4.4 The Monolith of PMMA/Silica Nanocomposites synthesized in Supercritical Carbon Dioxide

Polymer monolith is known as cross-linked polymer forming interconnected porous structures with the shape and dimension conforms to the closed mold where the polymerization takes place. Continuous monoliths have the flexibility offer open channels of various sizes allowing the mobile phase to pass through and thus can be used as high performance membrane chromatography. The flexibility of being prepared to fit the designed shape and size according to the task demands features a great advantage over other materials.

Preparation of monoliths often involves polymerization in a mixture of multifunctional monomers, porogenic diluents, and other solvents to fine tune the systems so that the structures of solid polymers can maintain their homogeneity. Major challenges faced in the preparation in liquid solutions include: high sensitivity of porous structure to porogneic diluents and solvents, volume shrinkage during polymerization, changes of structures or crack after the removal of solvents, and large amount of organic solvents required. During the last decade, the supercritical carbon dioxide has been used to replace the organic solvents in polymer monolith synthesis or processing.

In this work, the synthesis of macroporous polymeric composite monoliths reinforced by surface-functionalized silica nano-particles in supercritical carbon dioxide is presented. The in-situ polymerization of MMA that encapsulated well-dispersed silica nano-particles produced a uniform monolith with interconnected pores in size of few microns. Surface-functionalized silica nano-particles were first to form encapsulated microspheres through in-situ polymerization and dispersed uniformly in the reactor, followed by a sol-gel transition in a later stage that formed cross-linked interconnected porous monoliths. Poly

(dimethyl siloxane) methacrylate (PDMS-MA) was used as the surfactant stabilizer to prevent dispersed PMMA colloids and nanocomposites from premature agglomeration. The critical point pressure of PMDS increases with the concentration of MMA in supercritical carbon dioxide. The origin of sol-gel transition is likely induced by the consumption of monomer which lowers the solvency power of the medium to pull out and swell the PDMS chains.

Monolith synthesis with in-situ polymerization was conducted inside the high-pressure reaction vessel. In each run, 2 ml of monomer MMA, 0.04 g of initiator AIBN, and PDMS-MA were premixed, followed by the dispersion of silica nano-particles in the mixture. After purging with low-pressure carbon dioxide for five minutes, liquefied carbon dioxide was pumped into the reactor at room temperature until an appropriate pressure was reached. Before the reaction started, the monomer, stabilizer, and initiator were all dissolved in carbon dioxide, while the silica nano-particles are uniformly suspended in the reactor vessel. The vessel was then heated to 65°C to initiate the free-radical polymerization when the pressure also reached its desired final value. The reactor remained closed during the experiment. After 24 hours, carbon dioxide was released and the reactor was cooled down to room temperature for sample collection.

SEM was employed to examine the surface morphology and microstructure of the polymer materials. The surface morphologies were found in Figure 4.5, Figure 4.10, and Figure 4.11. A summary of the morphology according to various nanoparticle filler and surfactant concentrations is listed in Table 4.4 from which the only experiment configurations that lead to interconnected macroporous monolith are 10 % silica synthesized with 20 vol. % surfactant (Figure 4.5 (a) and (b), and 20 % silica synthesized with 20 vol. % surfactant (Figure 4.10 (g) and (h)). The morphology of the monolith samples show an interconnected macroporous

structure filling up uniformly the entire space of the mold. Encapsulated silica nano-particles can be seen from the surface morphology of the nanocomposites; no bare silica nano-particle was found excluded from the PMMA matrix.

The premise of fabricating monoliths of homogeneous structures is to have good dispersion of silica nano-particles in the reactor. The MPS-modified silica nano-particles were observed to disperse well in supercritical carbon dioxide due to the favorable interactions between MPS molecules and carbon dioxide. Upon gelation, the monoliths are strengthened by the interfusion of polymers and by the polymer-grafted silica particles, which are the "cross-linkers" throughout the polymer micro-domains. In this study, we demonstrate that the PMMA/silica nanocomposite monoliths could be synthesized with at least 10 wt. % silica nano-particles and 20 vol. % surfactant.

In principle, PMMA, PDMS, and PMMA-co-PDMS can tether to the silica nano-particle surface through the reaction with the surface vinyl groups. Tethered PMMA chains can greatly improve the dispersion of silica nano-particles in PMMA matrix. With the monomer co-solvent MMA, PDMS can provide adequate steric repulsions to prevent premature flocculation of the particles. The critical flocculation density (CFD) of supercritical carbon dioxide for the given PDMS has been regarded as a function of the MMA concentration under the given reaction conditions (Huang et al. 2001). At the early stage of the reaction, the medium carbon dioxide density is above CFD and PDMS can stabilize the particles effectively, however, as the conversion of MMA increases, CFD increases and eventually exceeds the medium density. The onset of gelation occurs when CFD is equal to the density of carbon dioxide and the dispersed colloids start to experience failure of stabilization and flocculate to form macroporous "gel". The chain length of PDMS and carbon dioxide pressure could be

used to adjust the onset of gelation. The kinetics of flocculation "reaction" against the diffusion of dispersed composite particles affects the porous structures. Recent neutron reflectivity study showed that bare silica surface has strong short-range attractive interactions with the siloxane groups of PDMS, which form a dense layer on the solid substrate even under high supercritical carbon dioxide density (Chen wt al., 2005). We believe that in our case, MPS and grafted PMMA have effectively screened such interactions. Upon gelation, the composites are strengthened by the interfusion of polymers and by the polymer-grafted silica particles, which are the "cross-linkers" throughout the polymer micro-domains.

Nano-particles with coronas of polymer brushes embedded in the composites should affect the mobility of PMMA even under carbon dioxide plasticization and retain the conformations after coagulations. Theoretically, surface-grafted PMMA/silica nanocomposites may have "bridge" and "loop" chain configurations when both ends of a chain are tethered to silica surface. Bridge configuration forms chemical cross-linking among distinct nano-particles; loop confiquration, on the other hand, featuring two ends tethered to the same particle, enhances polymer entanglements and decreases polymer mobility. A lower mobility lead to an increase of the characteristic "reaction time" for flocculation during the sol-gel process and also facilitates the stabilization of the composites from further structural changes. In order to verify polymer grafting and cross-linking, the PMMA/silica nanocomposites were repeatedly washed in excessive THF under supersonic bath for 2 hours to remove physically attached PMMA. Figure 4.14 depicts the SEM micrographs of the residuals after the filtration showing grafted polymer layers remained on the silica surface and small clusters of agglomerated nano-particles. These clusters, withstanding repeated dissolution and sonication, demonstrated strong cross-linkage among the silica nano-particles. Note that some dispersed

single nano-particles and small clusters were carried away by the solvent during the filtration and were not seen in the micrographs.

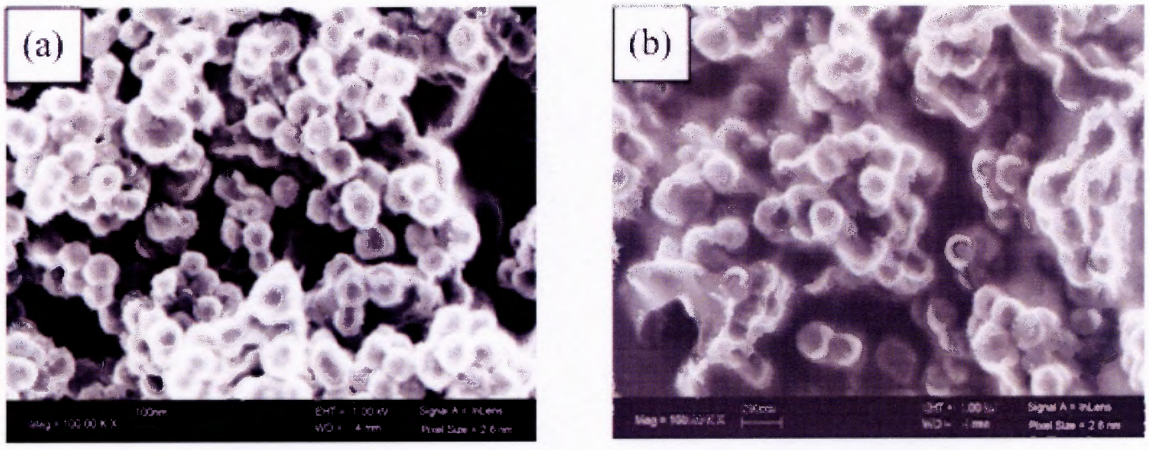

Figure 4.14 SEM micrographs of PMMA composite prepared from 75nm silica after 2 hours washes with THF in a supersonic bath. Images are taken after (a) the first wash, and (b) the second wash.

Table 4.4 Surface morphology obtained from SEM for samples synthesized with various surfactant and filler concentrations. (* was obtained from B. Yue et al., 2005)

Surfactant Conc.(%) / Filler Conc. (%)	0 (%)	5 (%)	10 (%)	20 (%)
0 (%)	Heavily Coagulated Irregular Shape			Agglomerate Spheres
5 (%)		Discrete Composite Spheres		Loosely Agglomerate Composite Sphere (*)
10 (%)	Coagulated Irregular Shape	Discrete Composite Spheres	Discrete Composite Spheres	Monolith
20 (%)				Monolith

4.5 Characterization of PMMA/Silica Nanocomposites Synthesized in Supercritical Carbon Dioxide Compared with Melt Mixing PMMA/Silica Nanocomposites

Thermal stability and mechanical properties of polymeric nanocomposites consisting of functionalized silica nano-particles (average diameter 75nm) embedded in polymethyl methacrylate (PMMA), with and without surface grafting of PMMA, were studied. Four samples were prepared for the comparative study: sample **1**, laboratory- grade PMMA, sample **2,** PMMA blended with unmodified silica nano-particles, sample **3**, PMMA blended with surface modified silica nano-particles, and sample **4**, PMMA/silica nanocomposites with grafted PMMA. Each composites contained 10 wt. % of silica nano-particles with PMMA of the same molecular weight.

In this section, the following investigations are reported:

1) Examine the thermal stability of samples **1**, **2**, **3**, and **4** by thermogravimetric analysis.

2) Examine the thermal stability of samples **1**, **2**, **3**, and **4** by differential scanning calorimetry analysis.

3) Examine the dynamic mechanical properties of samples **1**, **2**, **3**, and **4** by dynamic mechanical thermal analysis.

4.5.1 Thermogravimetric Analysis (TGA)

Figure 4.15 depicts the TGA results of weight loss percentage (%) versus temperature (^{o}C) of the samples. The weight loss profile of TGA could be roughly divided into three stages. The first stage, denoting the temperature range between 25–220°C with a weight loss of about 3%, is attributed to the loss of water and low boiling point organic residues. The second stage, a

significant weight loss of about 90% in the range of 220–440°C of **2**, **3** and **4**, and about 100% weight loss of **1** is attributed to the decomposition of PMMA. The third stage, featuring no weight loss between 440 and 475°C, is related to the presence of 10% nano-particle silica.

Quantitatively, the heat decomposition temperature (Td), defined as the temperature at 10% weight losses, increases from 260°C (**1**), 274°C (**2**), to 287°C (**3**). This is attributed to the presence of silica nano-particles and the improved coupling at the polymer/silica interface. Similar result was found as Chang et al. (2002) and Kim et al. (2003). However, the Td of **4** (243°C) was the lowest one. It may result from some PMMA chains of low molecular weight. Fig. 4.16 shows the molecular weight distribution (polydispersity index=3.1) of sample **4** obtained by gel permeation chromatography (GPC).

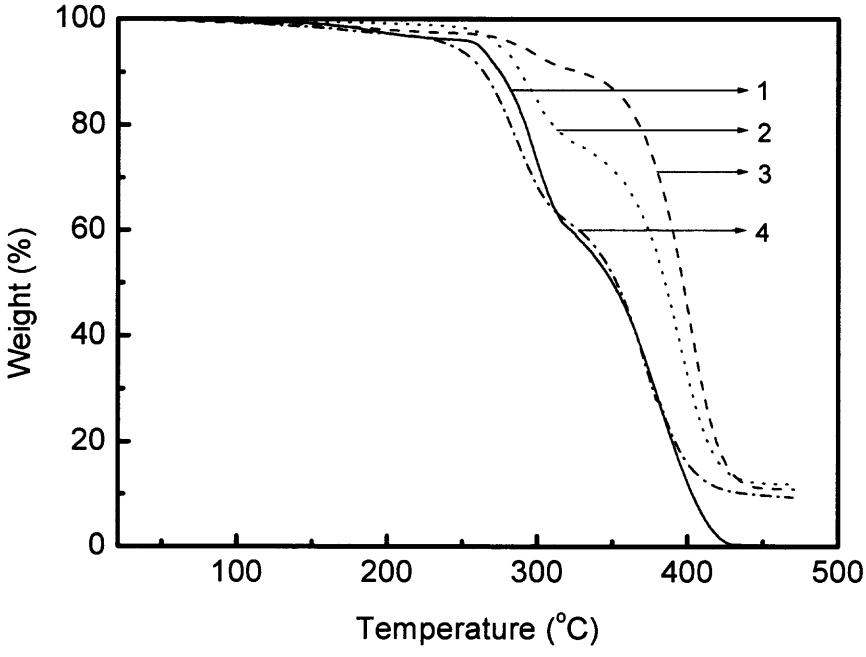

Figure 4.15 Weight loss percent vs. temperature plots of **1**, **2**, **3**, and **4** obtained from TGA (10°C/min).

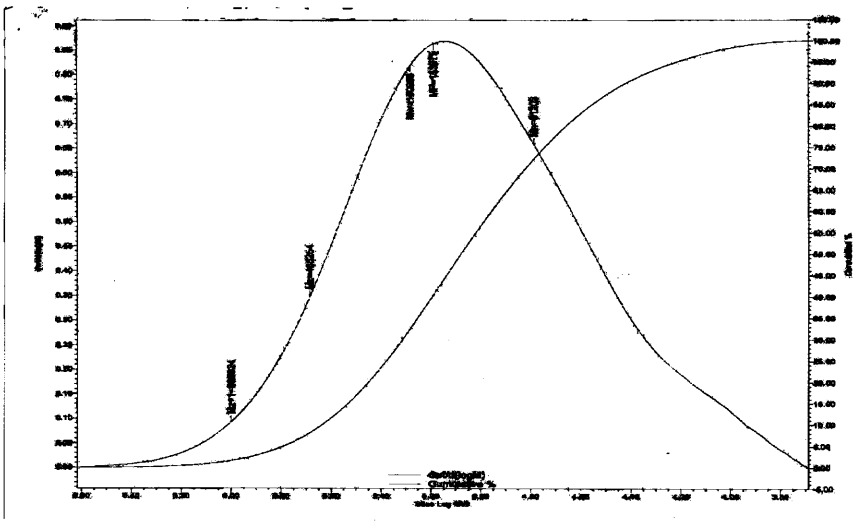

Figure 4.16 Molecular weight distribution of **4** obtained from GPC showing an average molecular weight of Mw=15,000 and PDI=3.1.

4.5.2 Differential Scanning Calorimetry Analysis (DSC)

Fig. 4.17 and Fig. 4.18 show the DSC thermograms of the samples during 1st cooling and 2nd heating cycles, respectively. From the cooling procedure, the glass transition temperature (T_g) of **1** is 117.04°C, which changes to 118.21°C in **2**, 118.73°C in **3** and 120.48°C in **4**. From the 2nd heating procedure, the T_g is 118.08°C in **1**, 121.59°C in **2**, 125.04°C in **3**, and 124.88°C in **4**; the T_g increases slightly from **1**, **2**, **3**, to **4**. The heat flow rates increase from **1**, **2**, **3**, to **4** during the cooling procedure; a similar result was observed during the heating procedure except that **3** had the highest heat absorption rate.

The DSC results have shown, to a noticeable extent, how the silica/polymer interfacial forces affect the mobility of polymer chains, and thus the T_g. Higher T_g enhances the thermal stability in certain applications. Similar result was found as Huang et al. (2003). Note that, in **4**, the silica/polymer interaction is the highest due to the grafting of PMMA onto the particle surface. The somewhat unexpected observation of similar T_gs in **3** and **4** may result from a

broader distribution of molecular weight in **4** and the existence of PDMS, which has a much lower T_g than PMMA and plasticizes the composites.

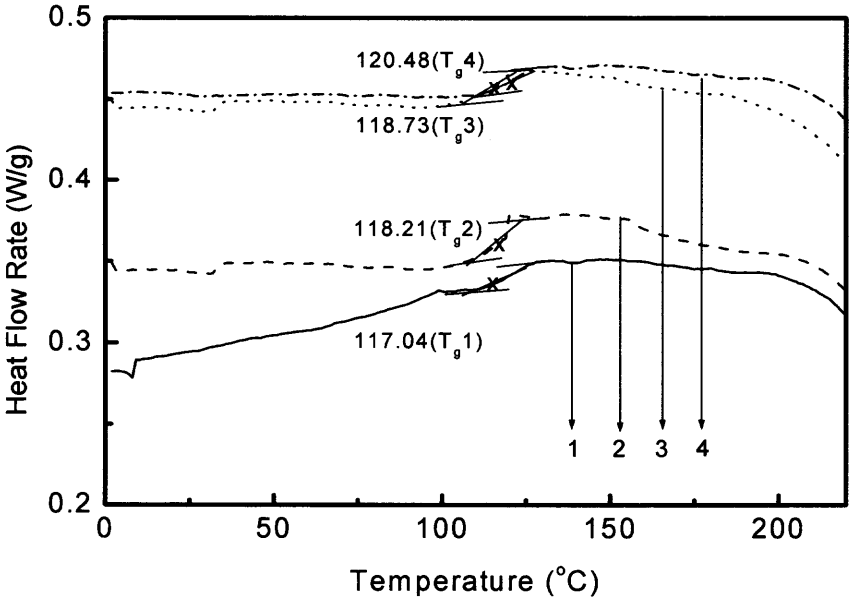

Figure 4.17 DSC results of the 1st cooling cycle (10°C/min) of **1**, **2**, **3**, and **4**.

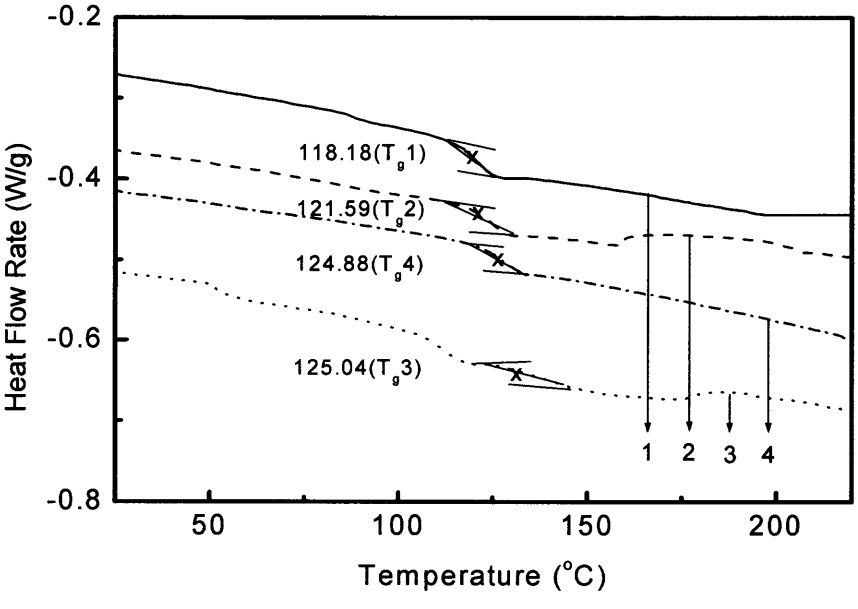

Figure 4.18 DSC results of the 2nd heating cycle (10°C/min) of **1**, **2**, **3** and **4**.

4.5.3 Dynamic Mechanical Thermal Analysis (DMTA)

Table 4.2 shows the samples dimensions and operating conditions for DMTA. Figure 4.19 depicts the change of storage modulus (E') with temperature (°C). The storage modulus increases from **1**, **2**, to **3** as the nano-particles and stronger interactions enhance the elasticity of the composites in the linear regime. However, the extent of increase is not significant. The second column of Table 4.3 depicts E' of the samples at 20°C; only less than 5% of increases in E' for composites **2** and **3** compared to **1** is observed. From the same column of Table 4.3 and Figure 4.16, the storage modulus of **4** is formed to be two orders of magnitude *lower* than **1**. The grafting of PMMA seems to lead to an opposite result than what was expected.

Figure 4.20 depicts the DMTA results of the loss modulus (E") against the temperature. The temperature at the peak position of the loss modulus increases from **1**, **2**, to **3** as the nano-particles restrain the collective motions of polymer and shift the dissipative responses towards a higher temperature. Comparing the temperatures corresponding to the peak positions, an increase of 10°C from **1** to **3** is observed. The loss modulus of **4** is again smaller than those of other samples by an order of magnitude.

Figure 4.21 displays the loss tangent (tan δ = E"/E') vs. temperature. Glass transition temperatures can be identified from the peak positions of the tan δ curves. It is found that T_g changes from 120°C in **1** to 121°C in **2**, 124°C in **3**, and 122°C in **4**, though this shift of the glass transition is not significant. Note that there is about 50% decrease in the heights of tan δ peaks from **1** to **3** due to the presence of silica nano-particles and their interactions. Decrease in tan δ may reflect the reduced mobility of the polymer chains as well as the intrinsic nature stemmed from the dispersed colloidal particulates. Similar results were found by M.

Kalogeras (2003). Though the Mw. of PMMA in **4** was the same as in **1-3** (Mw. =150,000). The tan δ of **4** exhibits an exceptional high value compared to other samples which may be attributed to the low T_g of PDMS-MA. PDMS is liquid at room temperature and becomes a plasticizer in the PMMA matrix.

Table 4.5 Sample Dimensions and Operating Conditions for DMTA

Sample	Thickness (mm)	Width (mm)	Length (mm)	Initial Strain (%)	Heating Rate (°C/min)
1	0.4	7.25	15.0	0.1	10
2	0.4	7.25	15.0	0.1	10
3	0.4	7.25	15.0	0.1	10
4	1.5	7.25	15.0	0.1	10

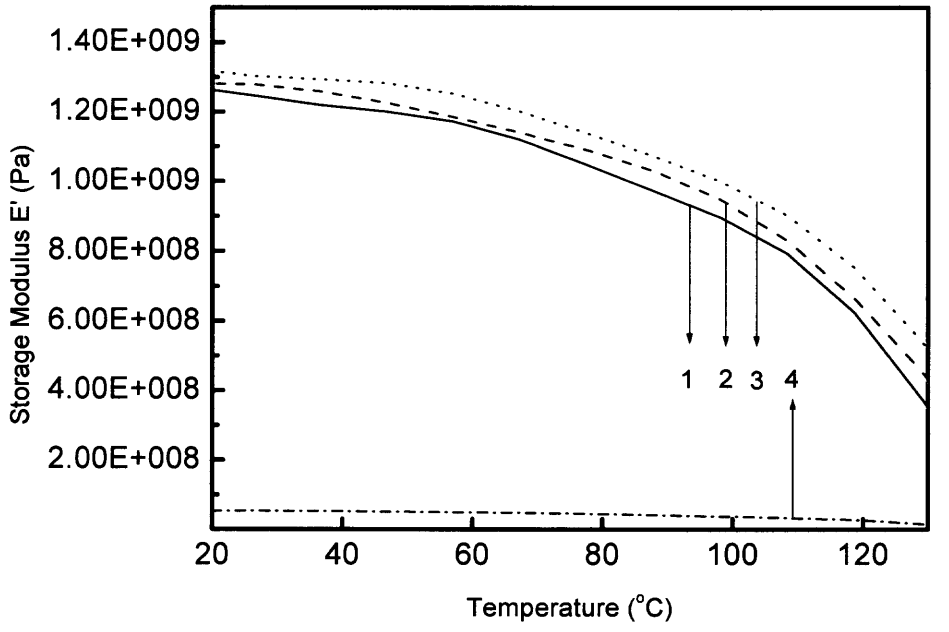

Figure 4.19 Storage modulus vs. temperature of **1, 2, 3,** and 4 obtained from DMTA.

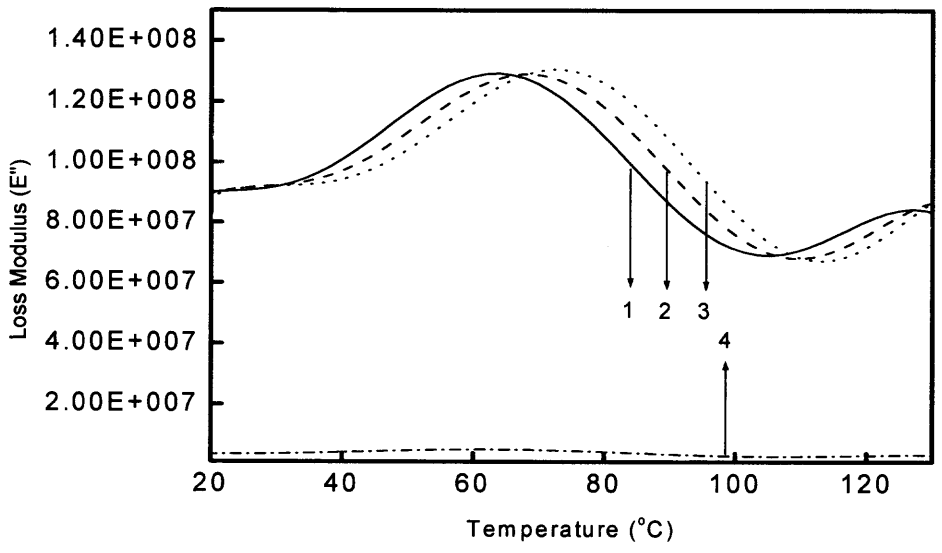

Figure 4.20 Loss modulus vs. temperature of **1, 2, 3,** and 4 obtained from DMTA.

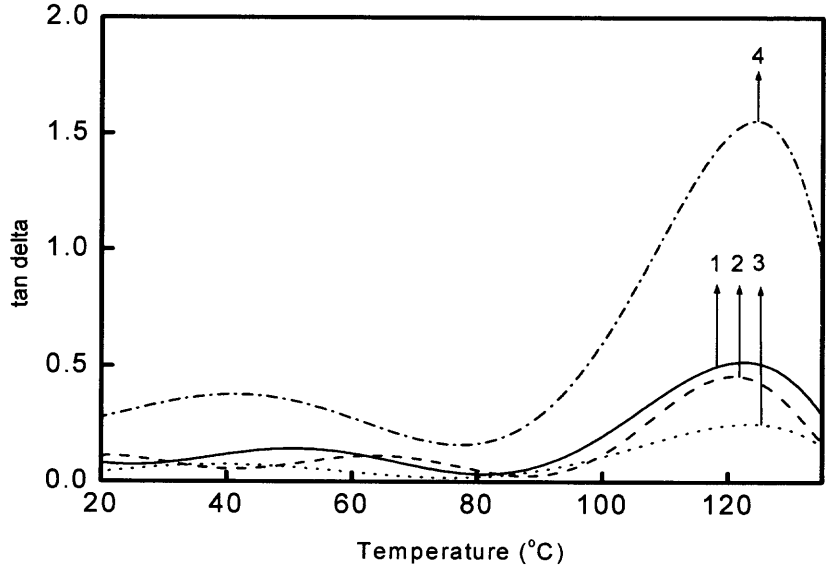

Figure 4.21 Loss tangent vs. temperature of samples **1**, **2**, **3**, and **4** obtained from DMTA.

Table 4.6 Results of DMTA

Sample	E' (Pa) , 20°C	E" (Pa) , 20°C	T_g from Loss Tangent (°C)
1	1.27×10^9	9×10^7	120
2	1.29×10^9	9.1×10^7	121
3	1.32×10^9	9.2×10^7	124
4	5.3×10^7	3.5×10^6	122

4.6 Characterization of PMMA/Iron Oxide Nanocomposites Synthesized in Supercritical Carbon Dioxide

Inclusion of magnetic nano-particles in polymers finds potential applications in spin-polarized devices, carriers for drug delivery, magnetic recording media, etc. However, for most of these specialized applications, dispersion of nano-particles in polymeric medium poses an important challenge. In this subsection, we synthesized first iron oxide nanoparticles with a dismeter of 35 nm. The nanoparticles were then used for the synthesis of nanocomposite monolith via in-situ polymerization in supercritical carbon dioxide.

4.6.1 Synthesis and Surface Functionalization of Iron Oxide Nano-particles

In the synthesis of iron oxide nano-particles, $FeCl_3 \cdot 6H_2O$ and $FeCl_2 \cdot 4H_2O$ black powders were dissolved in water with vigorous stirring followed by the addition of NH_4OH. An amount of 2.5 g of Dodecanedioic acid was added to the suspension and stirred at 90 °C for 30 min. The black water-based suspension was then cooled slowly to room temperature followed by the addition of perchloric acid in the solution. A black gum-like solid formed immediately that settled over a magnet, leaving a clear supernatant liquid with a thick surface scum of excess surfactant. The fluid with suspended black ferromagnetic particles becomes agitated when placed on the top of the device that generates rotating magnetic fields for stirring. The supernatant liquid was decanted, and the black residue was washed several times with acetone and methanol. The black precipitates were isolated from the solvent again by magnetic decantation. This washing-decantation procedure was repeated 5 times to remove the excess dodecanedioic acid used for the primary layer. Finally, the black precipitates were vacuum dried for 48 hours to obtain the surfactant-coated magnetic particles.

The magnetic particles synthesized by the above method are hydrophilic. To make the particle surface functionalized and hydrophobic, the ferromagnetic particles were added in a mixture of AEMA and DMF. The color of the solution changes from black to red immediately. The mixture was refluxed at 153 °C for 48 hours, and then was cooled down to 65 °C. After the reflux, the red solution was washed by THF with nano-filler to collect the ferromagnetic particles. The ferromagnetic particles can still respond to a magnetic field.

Figure 4.22 (a) depicts the scanning electron microscopy micrograph of iron oxide nano-particles which exhibit a near spherical shape and an average size of 35nm. Compared to the bare iron oxide particles, Figure 4.22 shows slightly irregular shapes for the particles functionalized with AEMA. Though loose agglomeration of the particles is observed in both the micrographs, we observed that AEMA-modified iron oxide dispersed very well in supercritical carbon dioxide even without stirring. This probably is due to the favorable interactions between AEMA molecules and MMA which facilitates the suspension in $ScCO_2$.

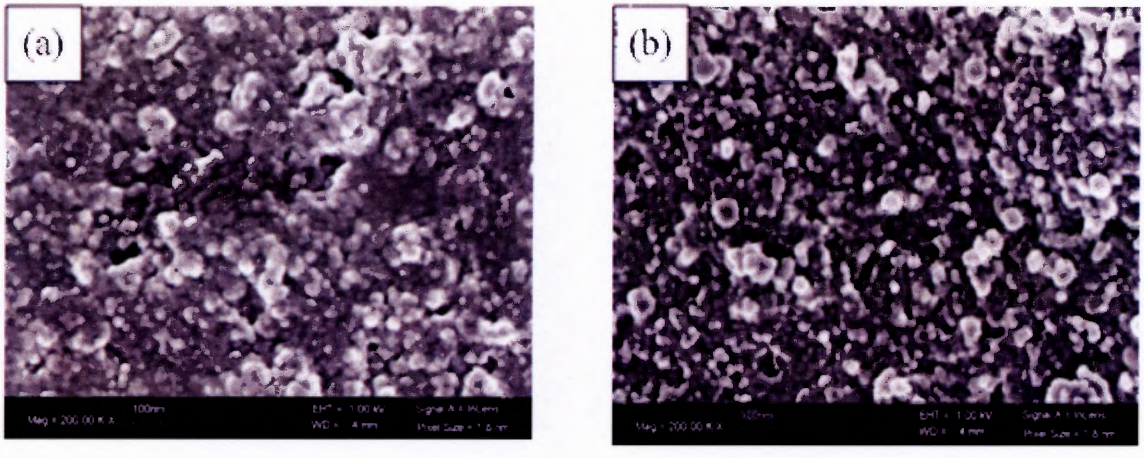

Figure 4.22 SEM images of (a) iron oxide particles (b) surface modified iron oxide particles with average size of 35 nm

4.6.2 Synthesis of PMMA/Iron Oxide Cross-linking Nanocomposite

Cross-linking is a process of chemically joining two or more molecules by a covalent bond. In this experimental study, bifunctional ethylene glycol dimethacrylate (EDMA) is used in the one-step reaction procedure.to cross-link PMMA and increases the mechanical strength of the nanocomposite. Before the polymerization, monomer MMA, 10 wt. % of surface modified iron oxide nano-particles, free-radical initiator, surfactant stabilizer, and cross-linker ethylene glycol dimethacrylate (EDMA) (how about toluene??) were premixed and charged into a small cylindrical mold placed in the reactor followed by purging with low-pressure carbon dioxide. The free-radical polymerization reaction was initiated and allowed to proceed for 24 hours at 65 ^{o}C in the reactor. Keep the reaction temperature at 65^{o}C and the vessel pressure at 27580 MPa for 24 hours. A chalk-like PMMA/iron oxide nanocomposite monolith was obtained as show in Figure 4.23.

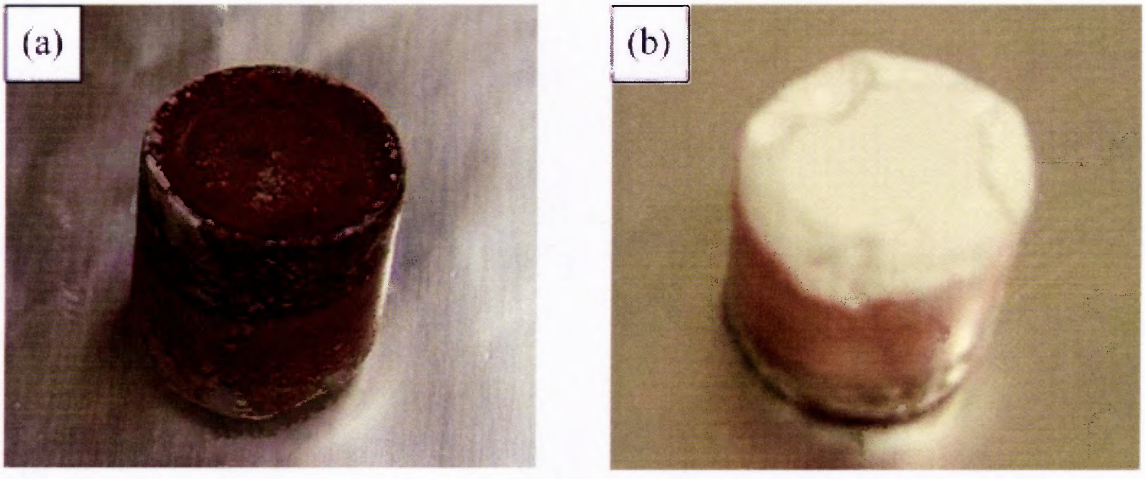

Figure 4.23 Macrographs of (a) and (b) PMMA/iron oxide nanocomposite monoliths prepared from 35nm iron oxide particles.

Figure 4.24 (a) and (b) depict the SEM micrographs of the macroporous monolith which consists of micron-sized polymeric nanocomposite particles that aggregate into an interconnected porous structure. Encapsulated iron oxide nano-particles can be seen from the surface morphology of the nanocomposites; no scattered bare iron oxide nano-particle was found excluded from the PMMA composites. The pore size distribution was in a range of few microns. Figure 4.24 (c), (d), (e), and (f) depict the surface morphology and the structures of the PMMA/iron oxide nanocomposites after a two-hour wash with THF. The micrographs of the residuals show the polymer layers remained on iron oxide surface and small clusters of agglomerated nano-particles. These clusters, withstanding repeated dissolution and sonication, demonstrated strong cross-linking among the iron oxide nano-particles. Note that some dispersed single nano-particles or small clusters were carried away by the solvent during the filtration and were not seen in the micrographs.

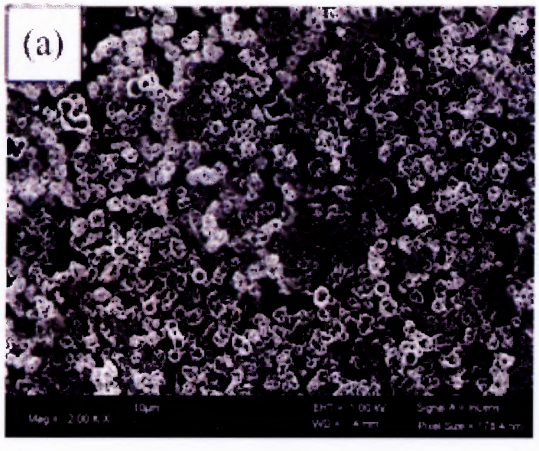

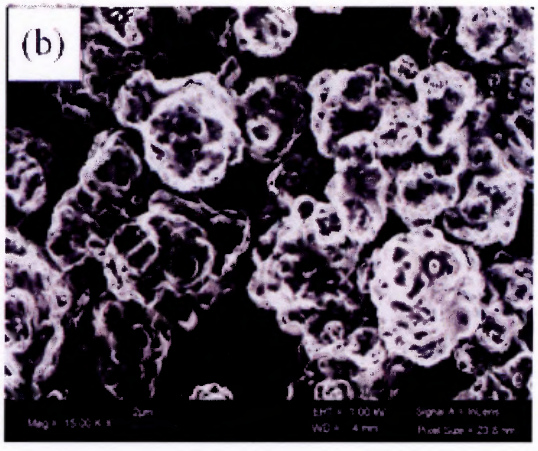

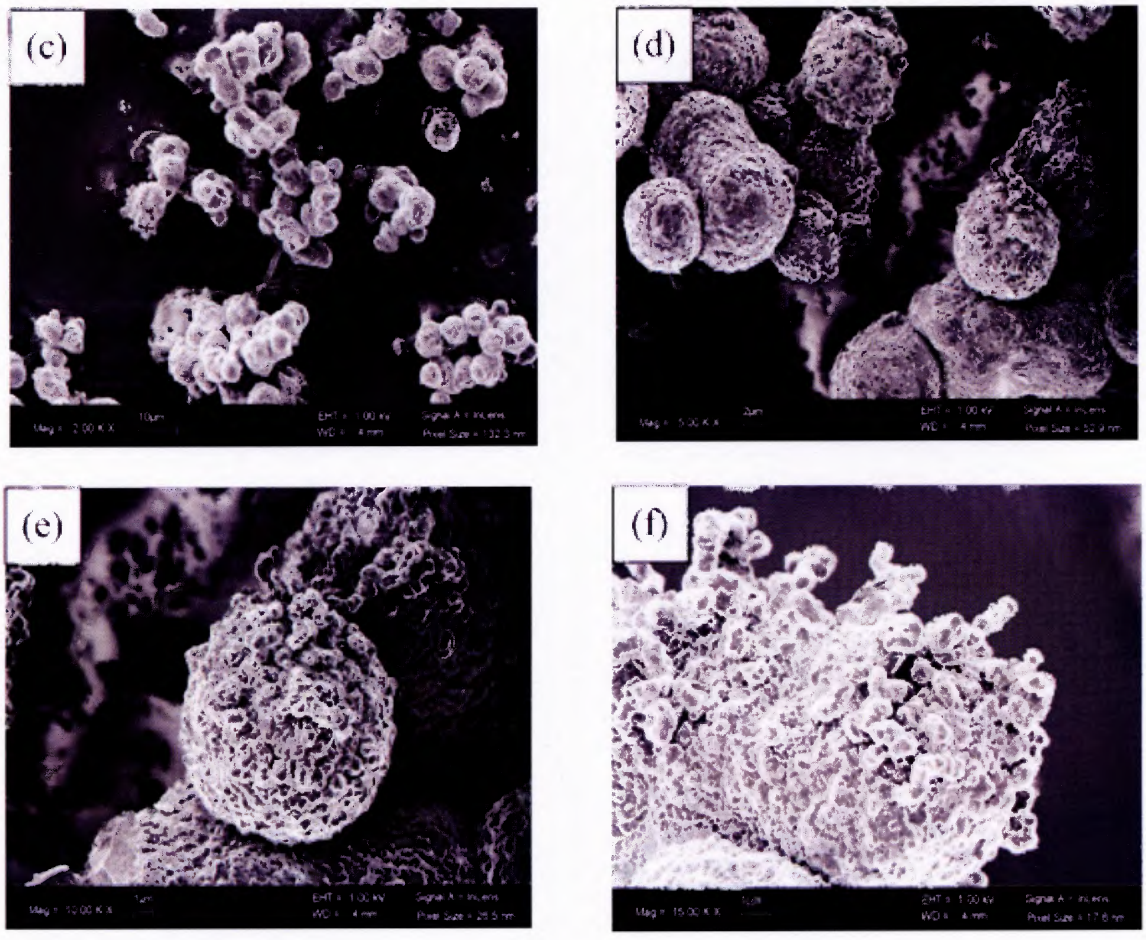

Figure 4.24 SEM images of (a) and (b) PMMA/ iron oxide nanocomposite monoliths containing the surface modified iron oxide particles prepared from 35nm iron oxide particles via in-situ polymerization in supercritical carbon dioxide, image of (b) is the magnification of (a). Images of (c), (d), (e), and (f) PMMA/ iron oxide nanocomposite monoliths prepared after 2 hours washed with THF in a supersonic bath, , images of (d), (e), and (f) are the magnification of (c).

4.6.3 Fourier Transform Infrared (FTIR)

Figure 4.25 shows the IR spectra of (a) synthesized iron oxide nano-particles, (b) functionalized iron oxide nano-particles, (c) PMMA/iron oxide nanocomposite monolith, and (d) PMMA/iron oxide nanocomposite monoliths after 2 hours washes with THF in a ultrasonic bath.

In Figure 4.25 (a), the -OH stretching peak at 3000~3600 cm^{-1} and the Fe_3O_4 stretching peaks at 575 $cm^{-1}$and 400 cm^{-1} show that the iron (II) chloride tetrahydrate and iron (III) chloride hexahydrate were hydrolyzed to form iron oxide nano-particles. The C-O stretching peak assigned at 1247 cm^{-1}, the C-H_2 stretching peak assigned at 1690 cm^{-1}, the C=C-COOH stretching peak assigned at 1690 cm^{-1}, and the C=O stretching peak assigned at 1730 cm^{-1} show that the iron oxide particle surfaces were functioned with -COOH groups by adding the dodecanoic acid.

In Figure 4.7 (b), the Fe_3O_4 stretching peaks at 575 $cm^{-1}$and 400 cm^{-1} show the presence of iron oxide nano-particles. The C-O stretching peak at 1247 cm^{-1}, the O=C-NH_2 stretching peak at 1630 cm^{-1}, and the C=O stretching peak at 1730 cm^{-1} demonstrate that, upon the addition of 2-Aminoethyl methacrylate hydrochloride and N, N,-dimethyl formamide, 2-Aminoethyl methacrylate hydrochloride has successfully reacted with the -COOH groups on the surface of the silica particles. In Figure 4.25 (c), the Fe_3O_4 stretching peaks at 575 $cm^{-1}$and 400 cm^{-1} show the presence of iron oxide particles. The Si-C stretching peaks at 1259 cm^{-1} show the presence of surfactant, PDMS-MA. The C-O stretching peak at 1247 cm^{-1}, the C=O stretching peak at 1730 cm^{-1}, and the C=C stretching peak at 1560 cm^{-1} indicate that the PMMA was synthesized. Figure 4.25 (d) shows the same peaks as those in figure 4.25 (c), indicative of that some PMA were chemically bonded to the surface of iron oxide particles after the removal of the physically attached PMMA from the nanocomposites.

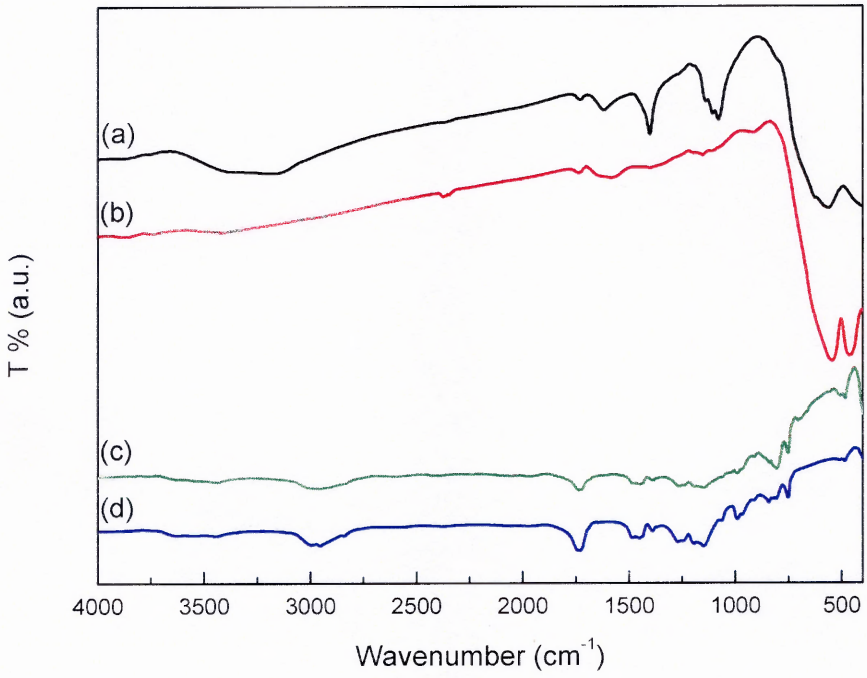

Figure 4.25 FTIR spectra of (a) synthesized iron oxide; (b) synthesized surface functionalized iron oxide; (c) PMMA/iron oxide nanocomposite monolith; (d) PMMA/iron oxide nanocomposite monolith after 2 hours washes with THF in a ultrasonic bath.

4.6.4 Thermogravimetric Analysis (TGA)

Figure 4.26 depicts the TGA results of weight loss percentage (%) versus temperature (°C) of PMMA/iron oxide nanocomposite. The weight loss profile of TGA could be roughly divided into three stages. The first stage, denoting the temperature range between 25–170°C with a weight loss of about 3%, is attributed to the loss of water and low boiling point organic residues. The second stage, a significant weight loss of about 90% in the range of 170–400°C is attributed to the decomposition of PMMA. The third stage, featuring no weight loss between 400 and 500°C, is related to the presence of iron oxide nano-particles.

Calculation from the TGA data shows that the real iron oxide nano-particle weight percentage in the sample is 8.7 %, which is comparable to the added filler amount of 10 %. Quantitatively, the heat decomposition temperature (Td), defined as the temperature at 10% weight losses, is 255°C. In comparison to the synthesized PMMA homopolymer, the decomposition temperature of PMMA/iron oxide nanocomposite increases from 235°C to 255°C due to the iron oxide fillers and the cross-linking agent enhanced the thermal stability of PMMA.

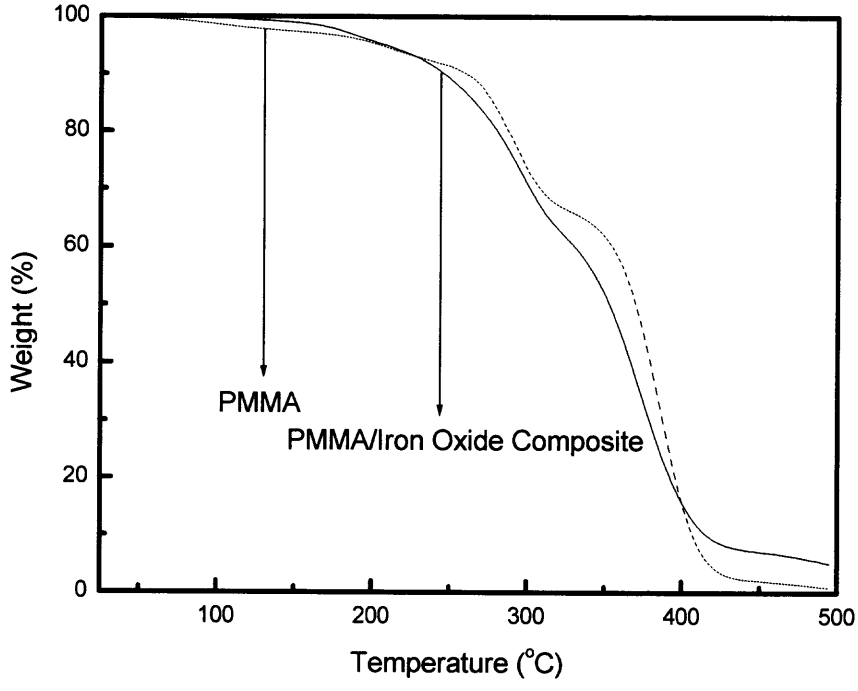

Figure 4.26 TGA (10°C/min) result of the weight percentage vs. temperature in PMMA/iron oxide nanocomposite containing 10 % iron oxide nano-particles.

4.6.5 Differential Scanning Calorimetry (DSC) Analysis

Fig. 4.27 shows the DSC thermograms of the sample during 1st cooling and 2nd heating cycles. From the cooling procedure, the glass transition temperature is 167.35°C. From the 2nd heating procedure, the glass transition temperature is 164.72°C. In comparison to the synthesized PMMA homopolymer and PMMA/silica nanocomposites, the glass transition temperature of PMMA/iron oxide nanocomposite increases around 50°C, resulting from the enhancement of cross-linking on the thermal stability of PMMA. Higher glass transition temperature enhances the thermal stability in certain applications.

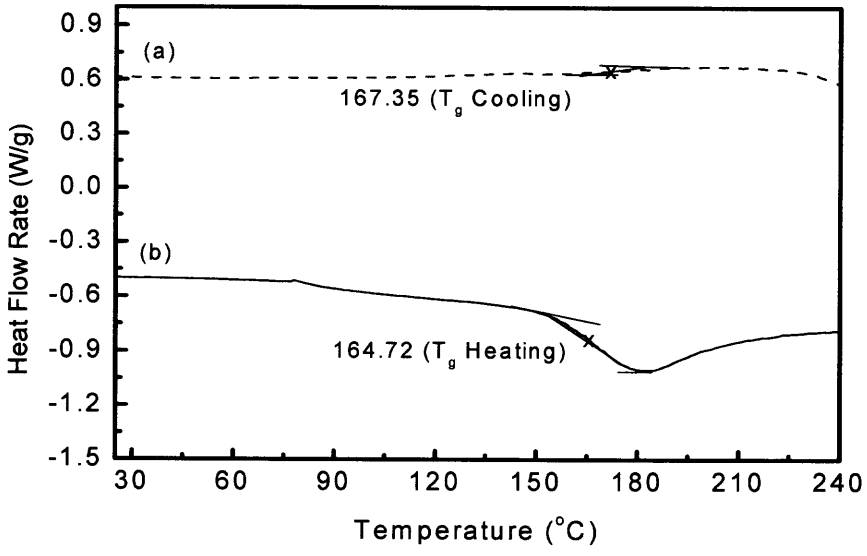

Figure 4.27 DSC results of (a) 1st cooling cycle (10°C/min) and (b) 2nd heating cycle (10°C/min) of PMMA/iron oxide nanocomposites containing 10 wt. % iron oxide nano-particles.

CHAPTER 5

CONCLUSIONS

Nanocomposites of PMMA and surface functionalized nanoparticle fillers including silica and ferromagnetic iron oxide were successfully prepared via in-site polymerization in supercritical carbon dioxide with PDMS-MA macromonomer as a surfactant stabilizer. Systematic study on the effects of the surfactant concentration and the weight ratio between the filler and the monomer showed a series changes in the morphology and the thermal stability. In general, higher surfactant concentration facilitated the dispersion of nano-particles in the polymeric composites; it also resulted in a higher number density of the polymeric nanocomposite particles. Excessive surfactant led to surface fusion of the polymeric composites due to the low Tg of PDMS. Without the surfactant, the inorganic filler could not be coated or encapsulated in PMMA. The observation suggested that the role of the surfactant does not only provide steric repulsion but also facilitated the deposition of precipitated polymer on the inorganic nanoparticle surface. It was also found that a higher content of inorganic nano-particles in the composites led to a higher number of nucleation sites and a finer structure in agglomeration. Within the range of the process variables studied in this thesis, only two configurations led to the formation of macroporous monolith: 20% of the surfactant concentration, 10% and 20% of the filler concentration.

DSC, TGA, and GPC data from this experiment showed that increasing surfactant concentration resulted in a higher polymer molecular weight,as well as higher glass transition temperature and decomposition temperature. The glass transition temperature also increased with the content of the nanoparticle filler due to the favorable interactions between the polymer

matrix and the functionalized nanoparticles. It was also found that the decomposition temperature increased with the content of inorganic nano-particles due to the formation of network structures in which the nanoparticles served as cross-linkers; the composites have much better thermal stability than PMMA homopolymer.

Thermal stability and mechanical properties of PMMA homopolymer, PMMA/silica melt mixing nanocomposites consisting of silica nano-particles, with and without surface grafting of PMMA, embedded in PMMA, and the PMMA/silica nanocomposites synthesized in supercritical carbon dioxide were studied. The TGA and DSC results showed better thermal stability of the PMMA/silica nanocomposites synthesized in supercritical carbon dioxide than others. The reason is that the PMMA/silica interaction is the highest due to the grafting of PMMA onto the silica particle surface. However, the surfactant, PDMS-MA, which has a very low Tg and is liquidus at room temperature became a plasticizer and resulted in poor mechanical property.

Polymeric nanocomposites of PMMA doped with iron oxide nano-particles were synthesized in supercritical carbon dioxide with the employment of cross-linking agent. In comparison to the synthesized PMMA homopolymer, an increase of decomposition temperature and the glass transition temperature was observed due to the formation of network structures caused by the fillers and the cross-linking agents.

REFERENCES

Calvo, L., Holmes, J.D., Yates, M.Z., and Johnston, K.P. (2000). Steric Stabilization of Inorganic Suspensions in Carbon Dioxide. Journal of Supercritical Fluids, 16, 247-251.

Chen, G., Chen, X., Lin, Z., Ye, W., and Yao, K. (1999). Preparation and Properties of PMMA/Clay Nanocomposite. Journal of Materials Science Letters, 18, 1761-1763.

Chen, M., Wu, L., Zhou, S., and You, B. (2005). Synthesis of Raspberry-Like PMMA/SiO2 Nanocomposite Particles via a Surfactant-Free Method. Macromolecules, 37, 9613-9619.

Chen, M., You, B., Zhou, S.-X., and Wu, L.-M. (2005). Preparation of Raspberry-like SiO2/PMMA Nanocomposite Spheres. Gaodeng Xuexiao Huaxue Xuebao/Chemical Journal of Chinese Universities, 26, 1352-1355.

Chen, W.C., and Lee, S.J. (2000). Synthesis and Optical Characteristics of Trialkoxycapped Poly (methyl methacrylate)-Silica Hybrid Films. Polymer Journal, 32, 67-80.

Chang, T.C., Wang, Y.T., Hong, Y.S., and Chiu, Y.S. (2000). Organic-Inorganic Hybrid Materials. V. Dynamics and Degradation of Poly(methyl methacrylate) Silica Hybrids. Journal of Polymer Science, Polymer Chemistry, 38, 1972-1980.

Choi, Y.S., Choi, M.H., Wang, K.H., Kim, S.O., Kim, Y.K., and Chung, I.J. (2002). Synthesis of Exfoliated PMMA/Na-MMT Nanocomposites via Soap-free Emulsion Polymerization. Macromolecules, 34, 8978-8985.

Choi, Y.S., Ham, H.T., and Chung, I.J. (2003). Polymer/Silicate Nanocomposites Synthesized with Potassium Persulfate at Room Temperature: Polymerization Mechanism, Characterization, and Mechanical Properties of the Nanocomposites. Polymer, 44, 8147-8154.

Choi, Y.S., Kim, Y.K., and Chung, I.J. (2003). Poly(methyl methacrylate-co-styrene)/Silicate Nanocomposites Synthesized by Multistep Emulsion Polymerization. Macromolecular Research, 11, 418-424.

Christain, P., Giles, M.R., Griffiths, R.T., Irvine, D.J., Major, R.C., and Howdle, S.M. (2000). Free Radial Polymerization of Methyl Methacrylate in Supercritical Carbon Dioxide Using a Pseudo-Graft Stabilize: Effect of Monomer, Initiator, and Stabilizer Concentrations. Macromolecules, 33, 9222-9227.

Cooper, A.I. (2000). Polymer Synthesis and Processing Using Supercritical Carbon Dioxide. Journal of Material Chemistry, 10, 207-234.

Desimone, J.M., Guan,Z., and Elsbernd, C.S. (1992). Synthesis of Fluoropolymers in Supercritical Carbon Dioxide. Science, 257, 945-947.

Han, M.J., and Young, T.A. (2005). Preparation of Poly(methyl methacrylate)/Na-MMT Nanocomposites via In-Situ Polymerization with Macroazoinitiator. Macromolecular Research, 13, 102-106.

Hodge P., and Sherrington D.C. (1989). Synthesis and Separations using Functional Polymers. Wiley, 28, 383-384.

Huang, Z., Kilic,S., Xu, J., Enick,R.M., Beckman, E.J., Carr, A.J., Melendez, R.E., and Hamilton, A.D. (1999). The Gelation of CO_2: A Sustainable Route to the Creation of Microcellular Materials. Science, 286, 1540-1543.

Huang, Z.H., and Qiu, K.Y., (1997). Preparation and Properties of Poly (styrene-*co*-maleic anhydride) / Silica Hybrid Materials by the In Situ Sol-Gel Process. Polymer, 38, 1067-1074.

Huang, X., and Brittain, W.J. (2000). Synthesis of a PMMA-Layered Silicate Nanocomposite by Suspension Polymerization. American Chemical Society, Polymer Preprints, Division of Polymer Chemistry, 41, 521-522.

Huang, X., and Brittain, W.J. (2001). Synthesis and Characterization of PMMA Nanocomposites by Suspension and Emulsion Polymerization. Macromolecules, 34, 3255-3260.

Jash, P., and Wilkie, C.A. (2005). Effects of Surfactants on the Thermal and Fire Properties of Poly(methyl methacrylate)/Clay Nanocomposites. Polymer Degradation and Stability, 88, 401-406.

Jeong, H.M., and Lee, S.H. (2003). Properties of Waterborne Polyurethane/PMMA/Clay Hybrid Materials. Journal of Macromolecular Science – Physics, 42, 1153-1167.

Johnston, K.P., (1989). Supercritical fluid science and technology; ACS Symposium Series.

Kalogeras, I.M. (2003). Side-Chain Motions in Poly(methyl methacrylate) + SiO_2 Hosts of Fluorescent Dyes Studied by Thermally Stimulated Discharge Currents: Effects of Confinement and Blending. Polymer, 44, 4817-4827.

Kashiwagi, T., Morgan, A.B., Antonucci, J.M., VanLandingham, M.R., Harris Jr., R.H., Awad, W.H., and Shields, J.R. (2003). Thermal and Flammability Properties of a Silica-Poly(methylmethacrylate) Nanocomposite. Journal of Applied Polymer Science, 89, 2072-2078.

Kendall, J.L., Canelas, D.A., Yang, J.L., and DeSimone, J.M., (1999). Recent Developments in Materials Synthesis and Processing Using Supercritical CO_2 Chemistry Review, 99, 543-538.

Kim, S., Kim, E., Kim, S., and Kim, W., (2005). Encapsulation of Polypyrrole Chains Inside the Framework of an Ordered Mesoporous Carbon. Journal of Colloid and Interface Science, 292, 93-98.

Kim, S.S., Park, T.S., Shin, B.C., and Kim, Y.B. (2005). Polymethyl methacrylate/Montmorillonite Nanocomposite Beads through a Suspension Polymerization-Derived Process. Journal of Applied Polymer Science, 97, 2340-2349.

Kurian, M., Dasgupta, A., Galvin, M.E., Ziegler, C.R., and Beyer, F.L., (2006). A Novel Route to Inducing Disorder in Model Polymer-Layered Silicate Nanocomposites. Macromolecules, 39, 1864-1871.

Kumar, S., Jog, J.P., and Natarajan, U. (2003). Preparation and Characterization of Poly(methyl methacrylate)-Clay Nanocomposites via Melt Intercalation: The Effect of Organoclay on the Structure and Thermal Properties. Journal of Applied Polymer Science, 89, 1186-1194.

Lami, E.B., and Lang, J., (1998). Encapsulation of Inorganic Particles by Dispersion Polymerization in Polar Media. J. of Colloid and Interface Science, 197, 293-296.

Li, Y., Zhao, B., Xie, S., and Zhang, S. (2003). Synthesis and Properties of Poly(methyl methacrylate)/Montmorillonite (PMMA/MMT) Nanocomposites. Polymer International, 52, 892-898.

Lim, S.T., and Choi, H.J. (2004). Effects of Layered Silicate on Nanoscopic Internal Structure and Morphology in Polymer Blend. Materials Science Forum, 449-452 (II), 1205-1208.

Liu , Q., Ding , J., Chambers ,D.E., Debnath , S., Wunder, S.L., and Baran, G.R., (2001). Filler-Coupling Agent-Matrix Interactions in Silica/Polymethylmethacrylate Composites. Journal of Biomedical Materials Research, 57, 384-393.

Lora, M., and Kikic, I. (1999). Polymer Processing with Supercritical Fluids. Separation and Purification Methods, 28, 179-220.

Luna-Xavier, J.L., Guyot, A., and Bourgeat-Lami, E. (2004). Synthesis and Characterization of Silica/Poly (methyl methacrylate) Nanocomposite Latex Particles through Emulsion Polymerization using a Cationic Azo Initiator. Journal of Colloid and Interface Science, 250, 82-92.

Luna-Xavier, J.L., Guyot, A., and Bourgeat-Lami, E. (2004). Preparation of Nano-sized Silica/Poly(methyl methacrylate) Composite Latexes by Heterocoagulation: Comparison of Three Synthetic Routes. Polymer International, 53, 609-617.

Manninen, A., Naguib, H.E., Nawaby, A.V., Liao, X., and Day, M. (2004). Effect of Clay Content on the Thermal and Physical Characteristics of PMMA Nanocomposite Foams. International Conference on Thermoplastic Foam Processing and Technology - Technical Papers, 95-100.

Manninen, A.R., Naguib, H.E., Nawaby, A.V., Liao, X., and Day, M. (2005). The Effect of Clay Content on PMMA-Clay Nanocomposite Foams. Cellular Polymers, 24, 49-70.

Manring, L.E., (1988).Thermal Degradation of Saturated Poly (methy1methacrylate). Macromolecules, 21, 528-530.

Manring, L.E. (1989). Thermal Degradation of Poly (methy1 methacrylate). 2. Vinyl-Terminated Polymer. Macromolecules, 22, 2673-2677.

Manring, L.E., Sogah, D.Y., and Cohen, G.M. (1989). Thermal Degradation of Poly (methy1 methacrylate). Macromolecules, 22, 4652-4654.

Meneghetti, P., Qutubuddin, S., and Webber, A. (2004). Synthesis of Polymer Gel Electrolyte with High Molecular Weight Poly(methyl methacrylate)-Clay Nanocomposite. Electrochimica Acta, 49, 4923-4931.

Meneghetti, P., and Qutubuddin, S. (2005). Application of Mean-Field Model of Polymer Melt Intercalation in Organo-Silicates for Nanocomposites. Journal of Colloid and Interface Science, 288, 387-389.

Meneghetti, P., and Qutubuddin, S., (2006). Synthesis, Thermal Properties and Applications of Polymer-Clay Nanocomposites. Thermochimica Acta, 442, 74-77.

Mori, Y., and Saito, R. (2004). Synthesis of a Poly(methyl methacrylate)/Silica Nano-Composite by Soaking of a Microphase Separated Polymer Film into a Perhydropolysilazane Solution. Polymer, 45, 95-100.

Okamoto, M., Morita, S., Kim, Y.H., Kotaka, T., and Tateyama, H. (2000). Synthesis and Structure of Smectic Clay/Poly(methyl methacrylate) and Clay/Polystyrene Nanocomposites via In-Situ Intercalative Polymerization. Polymer, 41, 3887-3890.

Okamoto, M., Morita, S., and Kotaka, T. (2000). Dispersed Structure and Ionic Conductivity of Smectic Clay/Polymer Nanocomposites. Polymer, 42, 2685-2688.

Okamoto, M., Morita, S., Kim, Y.H., Kotaka, T., and Tateyama, H. (2001). Dispersed Structure Change of Smectic Clay/Poly(methyl methacrylate) Nanocomposites by Copolymerization with Polar Comonomers. Polymer, 42, 1201-1206.

Parks, K.L., and Backman, E.J. (1996). Solubility, Diffusivity and Retrograde Vitrification in PMMA-CO_2..Polymer Engineering Science, 36, 2404-2408.

Qi, D.-M., Bao, Y.-Z., Huang, Z.-M., and Weng, Z.-X. (2006). Synthesis and Characterization of Poly(butylacrylate)/Silica and Poly(butyl acrylate)/Silica/Poly(methyl methacrylate) Composite Particles. Journal of Applied Polymer Science, 99, 3425-3432.

Qu, X., Guan, T., Liu, G., She, Q., and Zhang, L. (2005). Preparation, Structural Characterization, and Properties of Poly(methyl methacrylate)/Montmprillonite Nanocomposites by Bulk Polymerization. Journal of Applied Polymer Science, 97, 348-357.

Reverchon, E., Porta, G.D., Pace, S., Trolio, A.D. (1998). Supercritical Antisolvent Precipation of Submicronic Particles of Superconduct Precursors. Industry Engineering Chemistry Reservation, 37, 221-236.

Reverchon, E., Porta, G.D., Rosa, I.D., Subra, P., and Letourneur, D. (2000). Supercritical Antisolvent Micronization of Some Biopolymers. Journal of Supercritical Fluids, 18, 239-245.

Rhee, S.-H., and Choi, J.-Y. (2002). Synthesis of a Bioactive Poly(methyl methacrylate)/Silica Hybrid. Key Engineering Materials, 218-220, 433-436.

Salem, N., and Shipp, D.A. (2005). Polymer-Layered Silicate Nanocomposites Prepared through In-Situ Reversible Addition-Fragmentation Chain Transfer (RAFT) Polymerization. Polymer, 46, 8573-8581.

Sirard, S.M., Castellanos, H.J., Hwang, H.S., Lim, K-T., and Johnston, K.P. (2004). Steric Stabilization of Silica Colloids in Supercritical Carbon Dioxide. Industry Engineering Chemistry Reservation, 43, 525-531.

Stadtmueller, L.M., Ratinac, K.R., and Ringer, S.P. (2005). The Effects of Intragallery Polymerization on the Structure of PMMA-Clay Nanocomposites. Polymer, 46, 9574-9584.

Stober, W., Fink, A., and Bohn, A. (1968). Controlled Growth of Monodispersed Spheres in the Micron Size Range. Journal of Colloid and Interfacial Science, 26, 62-69.

Takahashi, H., Yamauchi, J., and Tomita, Y. (2005). Characterization of Silica-Nanoparticle-Dispersed Photopolymer Films that Include Poly(methyl methacrylate) as Host Binder Material. Japanese Journal of Applied Physics, Part 2: Letters, 44, L1008-L1010.

Tom, J.W., and Debenedetti, P.G. (1991). Formation of Bioerodible Polymer Microspheres and Microparticles by Rapid Expansion of Supercritical Solutions. Biotechnol. Progress, 7, 403-411.

Wang, H.-W., Shieh, C.-F., Chang, K.-C., and Chu, H.-C. (2005). Synthesis and Dielectric Properties of Poly(methyl methacrylate)-Clay Nanocomposite Materials. Journal of Applied Polymer Science, 97, 2175-2181.

Wang, H., Xu, P., Zhong, W., Shen, L., and Du, Q. (2005). Transparent Poly(methyl methacrylate)/Silica/Zirconia Nanocomposites with Excellent Thermal Stabilities. Polymer Degradation and Stability, 87, 319-327.

Wang, Y.-P., Pei, X.-W., Liu, X.-J., Kun-Yuan, Zhang, D.-X., Li, Q.-L., and Wang, Y.-F. (2005). Synthesis and Properties of Clay-Dispersed ABA Triblock Copolymer Nanocomposite via ATRP. Polymer Composites, 26, 465-469.

Wooding, A., Kilner, M., and Lambrick D.B. (1991). Studies of the Double Surfactant Layer Stabilization of Water-Based Magnetic Fluids. Journal of Colloid Interface Science, 144, 236-242.

Xie, T., Yang, G., Fang, X., and Ou, Y. (2003). Synthesis and Characterization of Poly(methyl methacrylate)/Montmorillonite Nanocomposites by In-Situ Bulk Polymerization. Journal of Applied Polymer Science, 89, 2256-2260.

Xu, M., Choi, Y.S., Wang, K.H., Kim, J.H., and Chung, I.J. (2003). Synthesis and Properties of Exfoliated Poly(methyl methacrylate-co- acrylonitrile)/Clay Nanocomposites via Emulsion Polymerization. Macromolecular Research, 11, 410-417.

Yang, F., and Nelson, G.L. (2004). PMMA/Silica Nanocomposite Studies: Synthesis and Properties. Journal of Applied Polymer Science, 91, 3844-3850.

Yates, M.Z., Shah, P.S., Johnston, K.P., Lim, K.T., and Webber, S. (2000). Steric Stabilization of Colloids by Poly (dimethylsiloxane) in Carbon Dioxide: Effect of Cosolvents. Journal of Colloid Interface Science, 227, 176-183.

Yeh, J.-M., Liou, S.-J., Lin, C.-Y., Cheng, C.-Y., Chang, Y.-W., and Lee, K.-R. (2002). Anticorrosively Enhanced PMMA-Clay Nanocomposite Materials with Quaternary Alkylphosphonium Salt as an Intercalating Agent. Chemistry of Materials, 14, 154-161.

Yeh, J.-M., Liou, S.-J., Lai, M.-C., Chang, Y.-W., Huang, C.-Y., Chen, C.-P., Jaw, J.-H., and, Yu, Y.-H. (2004). Comparative Studies of the Properties of Poly(methyl methacrylate)-Clay Nanocomposite Materials Prepared by In-Situ Emulsion Polymerization and Solution Dispersion. Journal of Applied Polymer Science, 94, 1936-1946.

Yu, Y.Y., Chen, C.Y., and Chen, W.C. (2003). Synthesis and Characterization of Organic–Inorganic Hybrid Thin Films from Poly (acrylic) and Monodispersed Colloidal Silica. Polymer, 44, 593-601.

Yeo, S.D., Lim, P.G., Debenedetti, P.G., and Bernstein, H. (1993). Formation of Microparticulate Protein Powders Using a Supercritical Fluid Anti-Solvent. Biotechnology Bioengineering, 41, 341-346.

Yue, B., Yang, J., Huang, C-Y, Dave, R., and Pfeffer, R. (2004). Synthesis of Macroporous PMMA/Silica Nanocomposite Monoliths in Supercritical Carbon Dioxide. Powder Technology, 16, 247-253.

Yue, B., Yang, J., Huang, C-Y, Dave, R., and Pfeffer, R. (2005). Synthesis of Macroporous PMMA/Silica Nanocomposite Monoliths in Supercritical Carbon Dioxide Macromolecular Rapid Community, 26, 1406-1411,

Zheng, X., Jiang, D.D., and Wilkie, C.A. (2005). Methyl Methacrylate Oligomerically-Modified Clay and its Poly(methyl methacrylate) Nanocomposites. Thermochimica Acta, 435, 202-208.

Zhang, W., Liang, Y., Luo, W., and Fang, Y. (2003). Effects of Clay-Modifying Agents on the Morphology and Properties of Poly(methyl methacrylate)/Clay Nanocomposites Synthesized via γ-Ray Irradiation Polymerization. Journal of Polymer Science, Part A: Polymer Chemistry, 41, 3218-3226.